CHALMERS
UNIVERSITY OF TECHNOLOGY

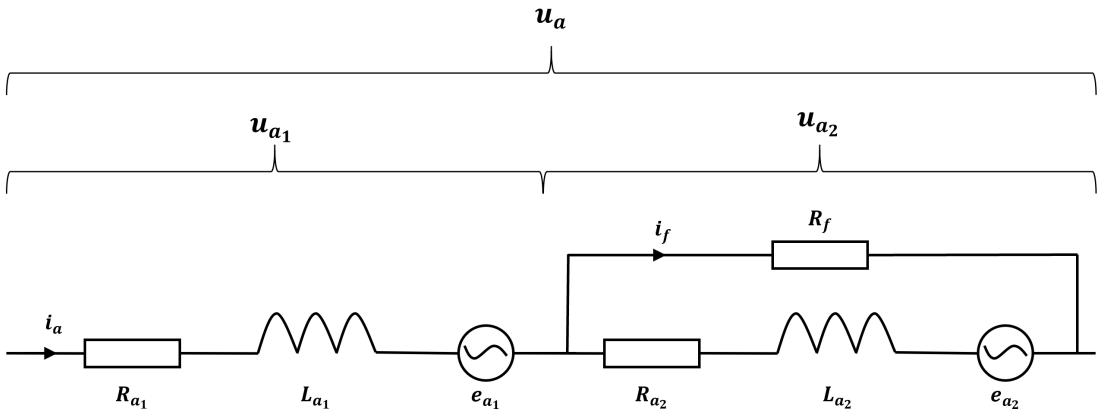

Detection of Stator Winding faults in Permanent Magnet Synchronous Machines

Master's thesis in Electric Power Engineering

SIMON OLOFSSON
ANTON GROTH

Department of Electrical Engineering
CHALMERS UNIVERSITY OF TECHNOLOGY
Gothenburg, Sweden 2019

Master's thesis 2019:NN

Detection of Stator Winding fault in Permanent Magnet Synchronous Machine

SIMON OLOFSSON
ANTON GROTH

CHALMERS
UNIVERSITY OF TECHNOLOGY

Department of Electrical Engineering
Division of Electric Power Engineering
Chalmers University of Technology
Gothenburg, Sweden 2019

Detection of Stator Winding fault in Permanent Magnet Synchronous Machine

ANTON GROTH
SIMON OLOFSSON

Supervisor: Ranjithh Raj Ram Prakash, AVL MTC Motortestcenter AB
Examiner: Stefan Lundberg, Department of Electrical Engineering

Master's Thesis 2019:NN
Department of Electrical Engineering
Division of Electric Power Engineering
Chalmers University of Technology
SE-412 96 Gothenburg
Telephone +46 31 772 1000

Cover: Equivalent circuit of a phase of a PMSM with a turn-to-turn fault

Typeset in LaTeX
Gothenburg, Sweden 2019

Detection of Stator Winding fault in Permanent Magnet Synchronous Machine

ANTON GROTH
SIMON OLOFSSON
Department of Electrical Engineering
Chalmers University of Technology

Abstract

The objective of this thesis is to detect turn-to-turn fault in the stator winding in a permanent magnet synchronous machine (PMSM) at an early stage before catastrophic failure. There are several different faults that can occur in a PMSM where the stator winding fault is the most common. The early stage of a stator winding fault is the turn-to-turn fault which will be the main focus. This fault is simulated by first designing a non-faulty PMSM model in SimuLink and Matlab and then expanding the model to behave like a faulty PMSM by adding fault turns. A non-faulted model is used as a benchmark to validate the accuracy of the faulted model. The PMSM is designed so that the fault severity can be varied by adjusting the number of turns shorted and the contact resistance between the shorted turns. To find a turn-to-turn fault different methods are considered and thoroughly discussed. The most suitable fault detection and diagnosis (FDD) methods, the motor current signature analysis (MCSA) and the zero sequence voltage component (ZSVC) are chosen due to their superior features. The MCSA is implemented with the simulated PMSM and produce satisfactory results. The results show that the FDD method can detect smaller faults such as turn-to-turn fault, which occur at an early stage, when R_f is approximately 27 Ω and the extra torque load is zero. When the extra torque load is 15 Nm the fault is detected at Rf 17 Ω. The ZSVC announces a fault when the zero sequence voltage reach a certain level which is not determined in the report. What is concluded is that the measured zero sequence voltage when a fault occurs is very low, around 1 mV, which makes it much more sensitive compared to the MCSA. Due to the sensitivity of the ZSVC and the simplicity of the MCSA, the MCSA is preferable.

Keywords: Permanent Magnet Synchronous Machine (PMSM), stator winding fault, turn-to-turn fault, fault detection, fault detection and diagnosis (FDD), Motor Current Signal Analysis (MCSA), zero sequence voltage component (ZSVC)

Acknowledgements

This master thesis has been conducted at AVL MTC Gothenburg during the year of 2019. Firstly we would like to thank our examinator Dr. Stefan Lundberg for his expertise, availability and understanding.
We would also like to thank Ranjithh Raj Ram Prakash at AVL MTC for his support and patience as our supervisor. We are also grateful to Björn Fager at AVL MTC for the opportunity to conduct our master thesis at AVL MTC. Finally, we would like to show gratitude to Dr. Torbjörn Thiringer for the guidance regarding software for out master thesis.

Anton Groth & Simon Olofsson
Gothenburg, Dec 2019

Contents

List of Figures

List of Tables

1

Introduction

1.1 Background

The demand for the PMSM (Permanent Magnet Synchronous Machine) is increasing due to its superior power density, higher efficiency and better power factor compared to the induction machine. The lower prices for rare-earth magnets is also a large contributor to PMSM's rising demand [1]. Failure of a PMSM can lead to loss of production time, expensive maintenance and even danger to personnel. Hence continuous and reliable operation is of the utmost importance.

In the PMSM faults occur both in the stator and the rotor. In the rotor faults such as demagnetising of the permanent magnets and damaged rotor bar are common. Demagnetising of the permanent magnets is when the magnets loose their magnetism for various reasons that occur over time [2]. A damaged rotor bar is when the rotor tooth get cracked or chipped due to wear [3].

One of the most common reason for a failure in the stator of the PMSM is the stator winding fault [14]. The stator winding fault occur when the winding insulation fails. When the insulation is worn down a short circuit current will occur between the windings, but also, depending on where the insulation has broken down, a phase-to-phase or phase-to-ground fault could occur. This short circuit current could be high enough to over time melt the windings themselves. This can further lead to more windings being short circuited, phase-to-ground fault and eventually even catastrophic failure. Methods of detecting a fault to prevent the electrical machine from a total failure can be done in different ways by using methods that monitor the different output signals of the machine.

The main goal with a FDD (Fault detection and diagnosis) method is to detect a fault before the performance of the machine is compromised. The absolute requirement is to detect the fault before the machine reach catastrophic failure. In some applications it is important to notice a fault at an early stage before they are close to compromise the performance of the machine. An example of this kind of application is the automotive industry, where performance issues will directly reduce the safety of the driver and other road-users. The automotive industry also have a need for online FDD as well as the possibility to find fault in a disruptive environment. A disruptive environment means that the signals such as mechanical torque, vibrations and acoustics might be difficult to read due to noise.

1.2 Aim

The aim for this thesis is to model and simulate a faulty PMSM for the automotive industry. The fault should then be detected by an FDD method at an early stage. To find a suitable FDD method to predict fault with, several different methods will be considered. The most suitable FDD methods will be implemented and tested to ensure their reliability.

1.3 Scope

The objective for this thesis is to develop a functional FDD method applicable for a PMSM in the automotive industry.

- Fault in the stator windings can occur in all electric motors but this thesis will only treat the PMSM due to its rising popularity and applicability in the automotive industry.
- The PMSM can have several different faults but this thesis will only consider the stator winding faults since its one of the most common fault amounting to around 35 % of all faults in electric machines [14][30].
- The PMSM will only be simulated and no experimental testing with physical components will be done.
- FDD methods that include machine learning will not be considered since there is a need for a large amount of data for both training and verification.
- FDD methods containing finite element analysis will be excluded due to high computing power.

1.4 Thesis outline

This thesis will consist of seven chapters. Chapter 2 will explain the PMSM model with equations. It will describe the non-faulty as well as the faulty model. The models will be compared to validate the faulted models accuracy. Chapter 3 will describe the FDD methods considered for this thesis. Where the FDD methods will be ranked and put into a table. The most relevant FDD methods will be explained in more detail and how they could be implemented. Chapter 4 will present the results with the chosen FDD methods. Chapter 5 will consist of a discussion regarding the results and chapter 6 will conclude the thesis. Lastly chapter 7 will present the part of the thesis that might be interesting for further work or studies.

2

Permanent Magnet Synchronous Machine

This chapter will describe how a non-faulted PMSM is modeled and how it can be expanded into a PMSM with a turn-to-turn stator winding fault. The most common stator windnig faults are the turn-to-turn fault [14]. The turn-to-turn fault occurs when an insulation breakdown happens between the windings. The insulation may breakdown due to stress from voltage, current and/or high temperatures. It may also breakdown due to aging of the material or mechanical stress. When the insulation is damaged a short circuit current occur between the windings that will stress the insulation even more due to high temperatures caused by the relatively high short circuit current which will lead to more turns being short circuited. The insulation between two phases could also breakdown. This is called a phase-to-phase fault and is considered severe since it could damage the machine permanently. The turn-to-turn fault could also happen in the stator housing which could eventually make the winding melt into the ground thus creating a direct contact between the phase and the ground, this is called a phase-to-ground fault. The phase-to-ground fault is dangerous to personnel since it will make the housing of the PMSM electrified [14].

2.1 Analytical PMSM model

This part of the chapter will present the general equations for a PMSM and the equations used to simulate a fault.

2.1.1 General PMSM model

In this section a general model of the PMSM is presented. The equations are acquired from [5]. The voltage in one phase, in this example phase a, can be expressed as

$$u_a = R_s i_a + \frac{d\Psi_a}{dt} \tag{2.1}$$

where u_a is the phase voltage, i_a is the phase current, Ψ_a is the phase flux linkage and R_s is the stator resistance which is equal in all three phases. The flux linkage contains the phase inductance and the back-EMF. The phase inductance is the sum of the self-induction and the mutual inductance and the back-EMF is the derivative of the magnetic flux. The phase voltage equation is then

$$u_a = R_s i_a + L_s \frac{di_a}{dt} + e_a \tag{2.2}$$

The equation applies to phase b and c as well. One phase can be represented as shown in Figure 2.1.

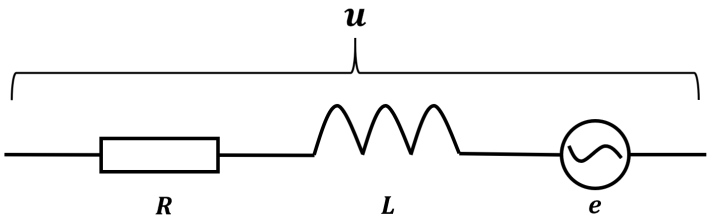

Figure 2.1: Circuit of one phase in the PMSM

To combine the phases a space vector for the voltage can be introduced similarly as done in [5],

$$u_s^s = R_s i_s^s + \frac{d\Psi_s^s}{dt} \tag{2.3}$$

Magnetic flux is a product of current and inductance, hence the flux linkage Ψ_s^s is a product of the current and the inductance in the phase plus the flux linkage coming from the rotor. The flux linkage can be expanded to

$$\Psi_s^s = L_s i_s^s + \Psi_m e^{j\phi_r} \tag{2.4}$$

where L_s is the stator self and mutual inductance, Ψ_m is the permanent magnet flux linkage and ϕ_r is the electrical rotor angle. Furthermore the time derivative of the electrical rotor angle is the electrical rotor speed, ω_r. Then the time derivative of (2.4) is

$$\frac{d\Psi_s^s}{dt} = L_s \frac{di_s^s}{dt} + j\omega_r \Psi_m e^{j\phi_r} \tag{2.5}$$

where $j\omega_r \Psi_m e^{j\phi_r}$ is the back-EMF of the machine. Combining (2.3) and (2.5) gives the general equation for a PMSM in stationary form

$$u_s^s = R_s i_s^s + L_s \frac{di_s^s}{dt} + j\omega_r \Psi_m e^{j\phi_r} \tag{2.6}$$

It can be observed that (2.6) is now very similar to (2.2).

In Figure 2.2 (2.6) is represented in a dynamical equivalent circuit.

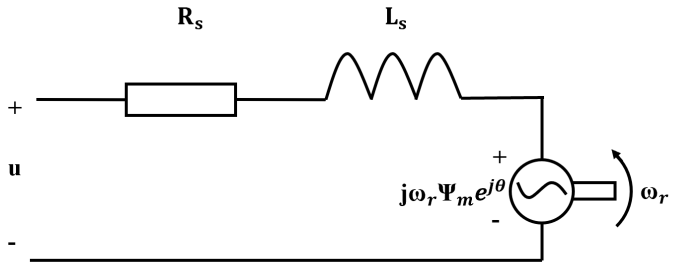

Figure 2.2: Dynamical equivalent circuit of a PMSM

To better analyze a PMSM the machine can be converted from stationary to rotating form. When doing so the following relations applies

$$i_s^s = i_s e^{j\theta_r}, u_s^s = u_s e^{j\theta_r}, \Psi_s^s = \Psi_s e^{j\theta_r} \tag{2.7}$$

where θ_r is the dq-transformation angle. Using the relations in (2.7) with (2.3) gives

$$u_s e^{j\theta_r} = R_s i_s e^{j\theta_r} + \frac{d}{dt}(\Psi_s e^{j\theta_r}) \tag{2.8}$$

where the derivative of $\Psi_s e^{j\theta_r}$ is

$$\frac{d}{dt}(\Psi_s e^{j\theta_r}) = \frac{d\Psi_s}{dt} e^{j\theta_r} + j\omega_r \Psi_s e^{j\theta_r} \tag{2.9}$$

Similarly, (2.4) becomes

$$\Psi_s e^{j\theta_r} = L_s i_s e^{j\theta_r} + \Psi_m e^{j\phi_r} \tag{2.10}$$

By assuming perfect field orientation, $\theta_r = \phi_r$, and combining (2.8) and (2.10) gives

$$u_s = (R_s + j\omega_r L_s) i_s + L_s \frac{di_s}{dt} + j\omega_r \Psi_m \tag{2.11}$$

which is the general equation for a PMSM in rotating form. Also worth noting is that $j\omega_r \Psi_m$ is the back-EMF. Equation (2.11) can be split into d and q, which gives

$$u_d = R_s i_d + L_d \frac{di_d}{dt} - \omega_r L_q i_q \tag{2.12}$$

$$u_q = R_s i_q + L_q \frac{di_q}{dt} + \omega_r L_d i_d + \omega_r \Psi_m \tag{2.13}$$

The PMSM can also be modeled in $\alpha\beta$-system. Equation (2.6) can be divided into a real and an imaginary part giving

$$u_\alpha = R_s i_\alpha + L_s \frac{di_\alpha}{dt} - \omega \Psi_m sin(\phi_r) \tag{2.14}$$

$$u_\beta = R_s i_\beta + L_s \frac{di_\beta}{dt} + \omega \Psi_m cos(\phi_r) \tag{2.15}$$

where $-\omega \Psi_m sin(\phi_r)$ is the back-EMF in α and $\omega \Psi_m cos(\phi_r)$ is the back-EMF in β. The speed of a PMSM is set by the number of poles in the rotor and the frequency of the supplied AC. The synchronous speed for the PMSM is

$$n_s = \frac{60 f_s}{n_p} \tag{2.16}$$

where f_s is the frequency of the supplied AC and n_p is the number of pole pairs. To the torque of a PMSM is calculated using the shaft power and the speed of the machine. The shaft power with amplitude invariant scaling is

$$P_e = \frac{3}{2} Re\{j\omega \Psi_m i_s^*\} = \frac{3\omega_r}{2} Im\{\Psi_m^* i_s\} \tag{2.17}$$

Using (2.17) assuming perfect field orientation the torque is

$$T_e = \frac{P_e}{\Omega_r} = \frac{n_p P_e}{\omega_r} = \frac{3\omega_r n_p}{2\omega_r} Im\{\Psi_s^* i_s\} = \frac{3n_p}{2}(\Psi_m i_q + (L_d - L_q) i_d i_q \tag{2.18}$$

where Ω_r is mechanical rotor speed which is $\Omega_r = \frac{\omega_r}{n_p}$. Another representation of the torque is done by using the back-emf as

$$P_e = T_e \Omega_r = e_a i_a + e_b i_b + e_c i_c \rightarrow T_e = \frac{e_a i_a + e_b i_b + e_c i_c}{\Omega_r} \tag{2.19}$$

where e_i is the back-emf for each phase.
To easily present the whole machine a matrix system is used by expanding (2.2) as

$$u_a = R_s i_a + L_a \frac{di_a}{dt} + M_{ab} \frac{di_b}{dt} + M_{ac} \frac{di_c}{dt} + e_a \tag{2.20}$$

where M_{ij} is the mutual inductance between the phases and e_a is the back-emf. Assuming that the machine is symmetrical the following is true

$$R_a = R_b = R_c = R_s \tag{2.21}$$

$$L_a = L_b = L_c = L_s \tag{2.22}$$

$$M_{ab} = M_{ac} = M_{bc} = M \tag{2.23}$$

Using the above relations and (2.20) a matrix representation of the machine can be done as

$$\begin{bmatrix} u_a \\ u_b \\ u_c \end{bmatrix} = \begin{bmatrix} R_s & 0 & 0 \\ 0 & R_s & 0 \\ 0 & 0 & R_s \end{bmatrix} \begin{bmatrix} i_a \\ i_b \\ i_c \end{bmatrix} + \begin{bmatrix} L_s & M & M \\ M & L_s & M \\ M & M & L_s \end{bmatrix} \frac{d}{dt} \begin{bmatrix} i_a \\ i_b \\ i_c \end{bmatrix} + \begin{bmatrix} e_a \\ e_b \\ e_c \end{bmatrix} \tag{2.24}$$

Matrix form can also be done in $\alpha\beta$

$$\begin{bmatrix} u_\alpha \\ u_\beta \end{bmatrix} = \begin{bmatrix} R_s & 0 \\ 0 & R_s \end{bmatrix} \begin{bmatrix} i_\alpha \\ i_\beta \end{bmatrix} + \begin{bmatrix} L_s & 0 \\ 0 & L_s \end{bmatrix} \frac{d}{dt} \begin{bmatrix} i_\alpha \\ i_\beta \end{bmatrix} + \begin{bmatrix} e_\alpha \\ e_\beta \end{bmatrix} \tag{2.25}$$

The mechanical part of the general PMSM model has three major quantities, the inertia of the machine, J, the mechanical or load torque, T_L, and the mechanical damping, B. These quantities are calculated with two different equations as

$$\frac{J}{n_p}\frac{d\omega_r}{dt} = T_e - T_L \tag{2.26}$$

The other equation is

$$T_L = B\Omega_r + T_{L,extra} \tag{2.27}$$

where $T_{L,extra}$ is a extra load added to the machine.

2.1.2 Faulty PMSM model

The equations for a faulty PMSM has been acquired from [6]. A turn-to-turn fault in a phase of a PMSM can be modelled as shown in Figure 2.3. As can be seen in the figure the phase is divided in two parts, one non-faulty, X_{a1}, and one with a turn-to-turn fault, X_{a2}. The fault insulation resistance between the turn-to-turn fault is modeled with the resistance R_f.

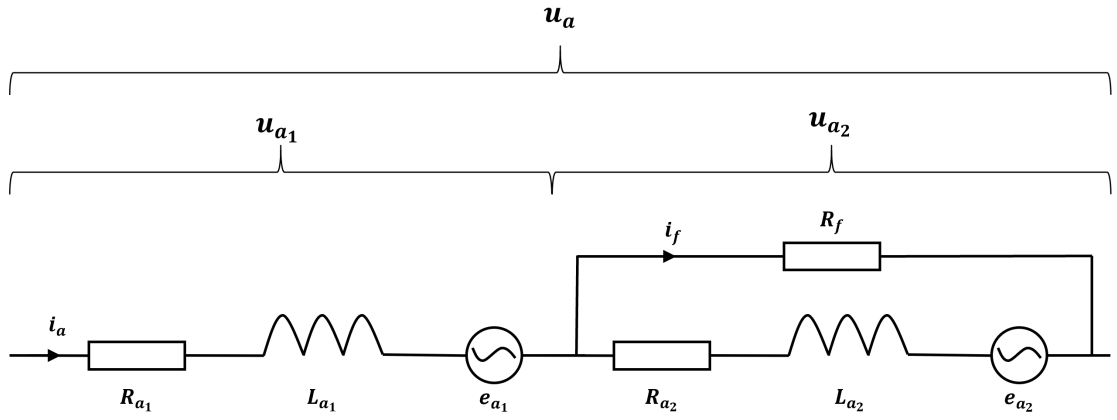

Figure 2.3: Circuit of a fault in phase a in the PMSM

The two voltages that appear in the faulted phase have the following equations

$$u_{a_1} = R_{a_1}i_a + L_{a_1}\frac{di_a}{dt} + M_{a_2a_1}\frac{d(i_a - i_f)}{dt} + M_{a_1b}\frac{di_b}{dt} + M_{a_1c}\frac{di_c}{dt} + e_{a_1} \tag{2.28}$$

$$u_{a_2} = R_{a_2}(i_a - i_f) + L_{a_2}\frac{d(i_a - i_f)}{dt} + M_{a_1a_2}\frac{di_a}{dt} + M_{a_2b}\frac{di_b}{dt} + M_{a_2c}\frac{di_c}{dt} + e_{a_2} \tag{2.29}$$

where i_f is the fault current, $M_{a_1a_2}$ is the mutual inductance between the two parts of the faulted phase and M_{a_xb} is the mutual inductance between each of the parts and the phases with no fault. R_f determines how good the contact is between the short circuited turns and can have a value from ∞ to 0. A low R_f results in a higher fault current and therefore a more severe fault. Since the machine is not altered in any way except adding a contact between the short-circuited turns the following can be assumed

$$u_a = u_{a_1} + u_{a_2}, \quad u_{a_2} = R_f i_f, \quad e_{a_2} = e_f, \quad R_a = R_{a1} + R_{a2} \tag{2.30}$$

Utilizing (2.28), (2.29) and (2.30) gives that u_a for the faulty phase is

$$u_a = R_a i_a + L_a \frac{di_a}{dt} + M_{ab}\frac{di_b}{dt} + M_{ac}\frac{di_c}{dt} + e_a - R_{a_2} i_f - (M_{a_2a_1} + L_{a_2})\frac{di_f}{dt} \quad (2.31)$$

Worth observing is that if i_f is equal to 0 equation the same as a healthy phase which means that the fault can be suppressed by setting R_f to ∞. The self-inductance ,L_a, is equal to the sum of the self-inductance and the mutual inductances between u_{a_1} and u_{a_2} which is [6]

$$L_a = L_{a_1} + L_{a_2} + M_{a_1a_2} + M_{a_2a_1} \quad (2.32)$$

Then considering that the machine is linear the mutual inductances between the two parts of the faulted phase and the non-faulted phases' is equal to the whole faulted phase and the non-faulted phases, as

$$M_{ab} = M_{a_1b} + M_{a_2b}, \quad M_{ac} = M_{a_1c} + M_{a_2c} \quad (2.33)$$

The short-circuit voltage, u_f, is then

$$u_f = 0 = (R_f + R_{a_2})i_f - R_{a_2} i_a + L_{a_2}\frac{di_f - i_a}{dt} - M_{a_1a_2}\frac{di_a}{dt} - M_{a_2b}\frac{di_b}{dt} - M_{a_2c}\frac{di_c}{dt} + e_{a_2} \quad (2.34)$$

From equation (2.31) and (2.34) the matrices for a faulted machine can be expressed as

$$\begin{bmatrix} u_a \\ u_b \\ u_c \\ 0 \end{bmatrix} = \begin{bmatrix} R_s & 0 & 0 & -R_{a_2} \\ 0 & R_s & 0 & 0 \\ 0 & 0 & R_s & 0 \\ -R_{a_2} & 0 & 0 & R_{a_2} + R_f \end{bmatrix} \begin{bmatrix} i_a \\ i_b \\ i_c \\ i_f \end{bmatrix} + \begin{bmatrix} L_s & M & M & -L_{a_2} - M_{a_1a_2} \\ M & L_s & M & -M_{a_2b} \\ M & M & L_s & -M_{a_2c} \\ -L_{a_2} - M_{a_1a_2} & -M_{a_2b} & -M_{a_2c} & L_{a_2} \end{bmatrix} \frac{d}{dt} \begin{bmatrix} i_a \\ i_b \\ i_c \\ i_f \end{bmatrix} + \begin{bmatrix} e_a \\ e_b \\ e_c \\ -e_f \end{bmatrix} \quad (2.35)$$

The matrices are modeled as (2.24) and the fault could be placed in any phase. Also worth observing is that if i_f=0 the matrices is equal to (2.24). This can also be written in $\alpha\beta$ like

$$\begin{bmatrix} u_\alpha \\ u_\beta \\ 0 \end{bmatrix} = \begin{bmatrix} R_s & 0 & 0 \\ 0 & R_s & 0 \\ -R'_{a_2} & 0 & R'_f \end{bmatrix} \begin{bmatrix} i_\alpha \\ i_\beta \\ i_f \end{bmatrix} + \begin{bmatrix} L'_s & 0 & L'_f \\ 0 & L'_s & 0 \\ -L'_f & 0 & L_{a_2} \end{bmatrix} \frac{d}{dt} \begin{bmatrix} i_\alpha \\ i_\beta \\ i_f \end{bmatrix} + \begin{bmatrix} e_\alpha \\ e_\beta \\ -e_f \end{bmatrix} \quad (2.36)$$

where

$$L'_s = L_a - M \quad (2.37)$$

$$R'_{a_2} = \sqrt{\frac{2}{3}} R_{a_2} \quad (2.38)$$

$$R'_f = R_{a_2} + R_f \quad (2.39)$$

$$L'_f = \sqrt{\frac{2}{3}}(L_{a_2} + M_{a_1a_2} - M_{a_2b}) \tag{2.40}$$

according to [6]. The electrical torque in abc and $\alpha\beta$ is, respectively

$$T_e = \frac{e_a i_a + e_b i_b + e_c i_c + e_f i_f}{\Omega_r} = \frac{e_\alpha i_\alpha + e_\beta i_\beta + e_f i_f}{\Omega_r} \tag{2.41}$$

To calculate the resistance and back-emf in the part of the phase where the fault occurs the variable μ is introduced. μ is a ratio between the faulted turns, N_f and the total number of stator turns, N_s, as

$$\mu = \frac{N_{a_2}}{N_s} = \frac{N_f}{N_s} \tag{2.42}$$

Then the equations for R_{a_2} and e_{a_s} is

$$R_{a_2} = \mu R_s \qquad e_{a_2} = e_f = \mu e_a \tag{2.43}$$

The same method is not preferred to use when calculating the inductances since the error between the calculated and actual value is too large [6]. For example, if the mutual inductance in the faulty phase would be scaled with μ the equation would be $M_{a_1a_2} = \mu(1-\mu)L_s$ where it can be seen that the mutual inductance will have a positive value, while it should be negative, since it is a mutual inductance, and the calculated value will be much higher than the actual value. In [6] the inductances calculated by scaling with μ were compared with inductances acquired with FEM. In Table 2.1 the difference that was observed is presented when $\mu = 50$ %.

Table 2.1: Comparison of inductances when calculated with μ-scaling, calculated utilizing individual coils and acquired with FEM. The values are taken form [6]

	L_{a_1}=L_{a_2}	$M_{a_1a_2}$	M_{a_2b}=M_{a_2c}
FEM	1.6	-0.19	-0.28
With μ	0.705	0.705	-0.14
With coils	1.62	-0.2	-0.15

The inductances can instead be calculated using the number of poles and fault turns. A machine have a number of bobbins or coils per phase in the stator. Using the coils, the number of faulted turns and the number of total turns the calculated value of the inductances are much more accurate than just using μ [6]. The general expression for the inductance of a phase for a healthy PMSM when calculating with the help of individual coils is

$$L_a = p(L_{coil} + (p-1)M_{coil}) \tag{2.44}$$

where L_a is the self-inductance of the whole phase, L_{coil} is the inductance for one coil, M_{coil} is the mutual inductance between two coils and p is the number of coils in one phase. A visual representation of this equation can be seen in Figure 2.4.

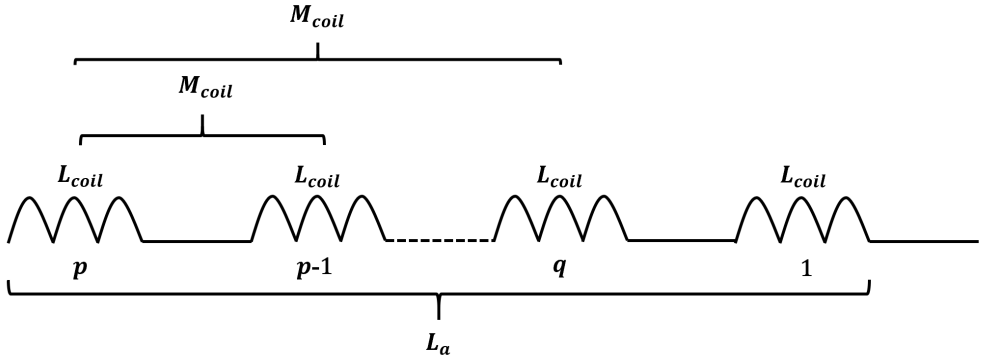

Figure 2.4: A visual representation of how L_{coil} and M_{coil}

To calculate the inductances in a PMSM with a fault a new variable is introduced, μ_{coil}, which is a ratio of number of fault turns over total number of turns in the affected coil. The equation for μ_{coil} is

$$\mu_{coil} = \frac{N_{f_{coil}}}{N_{coil}} \tag{2.45}$$

where $N_{f_{coil}}$ is number of fault turns in one coil and N_{coil} is number of total turns in one coil. The inductances of the faulty phase can then be calculated as

$$L_{a_1} = (p-q)(L_{coil}+(p-q-1)M_{coil})+(1-\mu_{coil})^2 L_{coil}+2(1-\mu_{coil})(p-q)M_{coil} \tag{2.46}$$

$$L_{a_2} = (q-1)(L_{coil}+(q-2)M_{coil})+\mu_{coil}^2 L_{coil}+2\mu_{coil}(q-1)M_{coil} \tag{2.47}$$

$$M_{a_1a_2} = (q-1)(p-q)M_{coil}+\mu_{coil}(p-q)M_{coil}+(1-\mu_{coil})(q-1)M_{coil}+\mu_{coil}(1-\mu_{coil})L_{coil} \tag{2.48}$$

where q dictates in which coil the faulty occurs. Figure 2.5 shows a simple circuit where a fault occurs in coil q, in this case the second to last coil, and 50 % of the affected coil is short circuited.

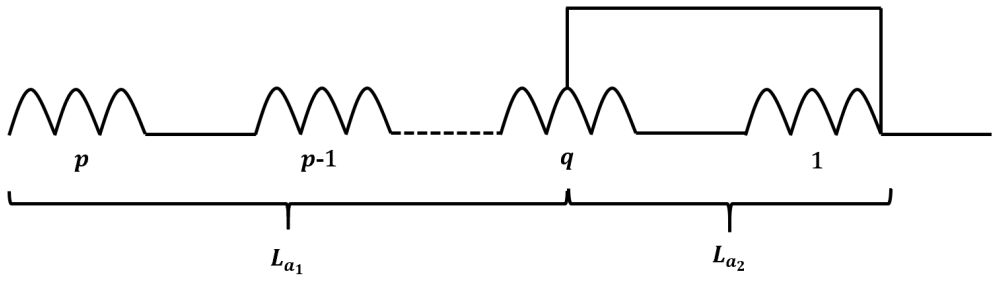

Figure 2.5: Representation of a fault. In the shown case μ_{coil} is 50 %

The self-inductance L_a is, as described earlier, the sum of the self-inductances and the mutual inductances

$$L_a = L_{a_1} + L_{a_2} + 2M_{a_1a_2} \tag{2.49}$$

2.1.3 State space equations

In this section the state space equations for both a faulted and non-faulted machine will be presented. The general state space model is

$$\begin{aligned} \frac{d\mathbf{x}}{dt} &= \mathbf{Ax+Bu} \\ \mathbf{y} &= \mathbf{Cx+Du} \end{aligned} \tag{2.50}$$

where $\mathbf{x}$ is the states, $\mathbf{u}$ is the inputs and $\mathbf{y}$ is the outputs. If $\mathbf{x}$=$[i_\alpha \quad i_\beta]^T$, the state space expression for (2.25) will be

$$\begin{aligned} u &= \begin{bmatrix} u_\alpha - e_\alpha & u_\beta - e_\beta \end{bmatrix}^T \\ A &= -\begin{bmatrix} L'_s & 0 \\ 0 & L'_s \end{bmatrix}^{-1} \begin{bmatrix} R_s & 0 \\ 0 & R_s \end{bmatrix} \\ B &= \begin{bmatrix} L'_s & 0 \\ 0 & L'_s \end{bmatrix}^{-1} \end{aligned} \tag{2.51}$$

The state space model for a faulty machine using (2.36) and setting the state variables to $x = [i_\alpha \quad i_\beta \quad i_f]^T$ is

$$\begin{aligned} u &= \begin{bmatrix} u_\alpha - e_\alpha & u_\beta - e_\beta & e_f \end{bmatrix}^T \\ A &= -\begin{bmatrix} L'_s & 0 & -L'_f \\ 0 & L'_s & 0 \\ -L'_f & 0 & L_{a_2} \end{bmatrix}^{-1} \begin{bmatrix} R_s & 0 & -R'_{a_2} \\ 0 & R_s & 0 \\ -R'_{a_2} & 0 & R'_f \end{bmatrix} \\ B &= \begin{bmatrix} L'_s & 0 & -L'_f \\ 0 & L'_s & 0 \\ -L'_f & 0 & L_{a_2} \end{bmatrix}^{-1} \end{aligned} \tag{2.52}$$

2.2 PMSM control system

This section will describe the control system used in the PMSM simulations. The control system was acquired from [5]. In Figure 2.6 a simplified block diagram of the whole control system is shown. The controller used in the simulations is a position-sensored vector control. The PMSM in the block diagram is the machine

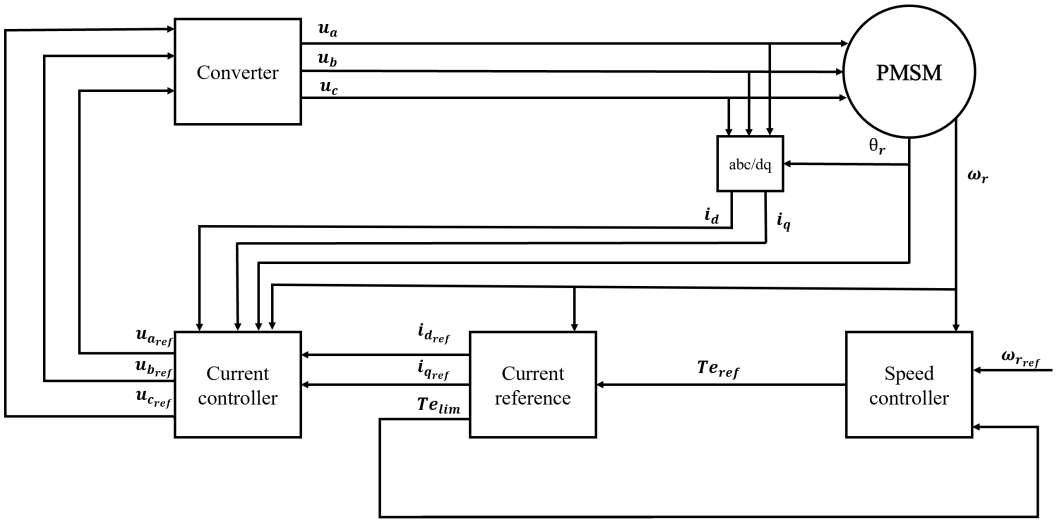

Figure 2.6: Block diagram of the control system for the PMSM

model derived in the previous sections. The controller then consists of three major blocks. Firstly a speed controller where speed from the machine, the reference speed and the limited electric torque is the inputs. The speed controller is a simple PI-controller that calculates the reference electric torque which is the only output from the speed controller. The reference electric torque act as the input to the current reference calculation block together with the actual speed of the machine. The current reference block calculates the reference current in dq-component form and also sends back the limited electric torque to the speed controller. The last block in the controller is the current controller which is two PI-controllers, one for i_q and one for i_q, that calculates the reference voltage in three phase representation. The inputs to the current controller is the reference current, the actual current and the actual speed. The three PI-controllers have different closed loop bandwidths where the two in the current controller has a closed loop bandwidth of 3000 rad/s while the speed controller only has one of 20 rad/s. This difference is due to the controller for the electrical part should be much faster since the system inertia of the electrical part compared to the mechanical part is much slower.

2.3 Setup of a PMSM with fault

This section will describe the approach taken in this report to simulate a PMSM with a fault. The machine used is acquired from [7] and its parameters can be found in Appendix A.1. From here on this machine will be referred to as the PMSM. Since

no FEM analysis will be conducted in the report an additional machine, obtained from [6], is used to calculate the fault inductances of the machine. The parameters for this machine can be found in Appendix A.2 and this machine will from here on be referred to as the reference PMSM.

2.3.1 Inductance calculation

As mentioned in section 2.1.2 the fault inductances need to be calculated more precise than just scaled with the help of μ. The inductances for a fault was calculated using (2.46), (2.47) and (2.48). Since the geometry in the two PMSMs are similar it is assumed that the self inductance and mutual inductance are proportional between the two different PMSMs. To obtain the values of L_{coil} and M_{coil} the reference machine was used as

$$M_{coil} = \frac{L_s}{p(\frac{L_{coil_{ref}}}{M_{coil_{ref}}} + (p-1))} \tag{2.53}$$

where p is the number of coils, $L_{coil_{ref}}$ and $M_{coil_{ref}}$ are from the reference PMSM and L_s is self inductance from the PMSM and M_{coil} is the inductance of one coil in the PMSM. Equation (2.53) is based on (2.44) and then modified so that it calculates M_{coil} for the PMSM. L_{coil} is then calculated using (2.44). The calculated L_{coil} and M_{coil} are presented in Appendix A.1. To obtain $L_{coil_{ref}}$ and $M_{coil_{ref}}$ (2.46) and (2.48) was used. Since L_s, L_{a_1}, $M_{a_1a_2}$, p, q and μ_{coil} are known and the only unknown are M_{coil} and L_{coil} it can be solved with a simple equation system.

2.3.2 PMSM model with fault

The simulation of a PMSM with inter-turn short circuit fault takes its base from a PMSM with no fault. This can easily be seen by comparing (2.51) and (2.52). The faulty machine consist of more parameters since the affected phase has been split into two parts as can be seen in section 2.1.2. To simulate different severity of the fault μ, μ_{coil} and R_f has been adjusted to see what has the most impact on the fault and if it can be noticed by a FDD-method. Since all simulations done in this report is only executed in Matlab and Simulink they are completely ideal. In Figure 2.7 the current of the faulty PMSM with a very large R_f, then acting as a non-faulty machine, can be seen and because of the ideal conditions all harmonics are practically negligible.

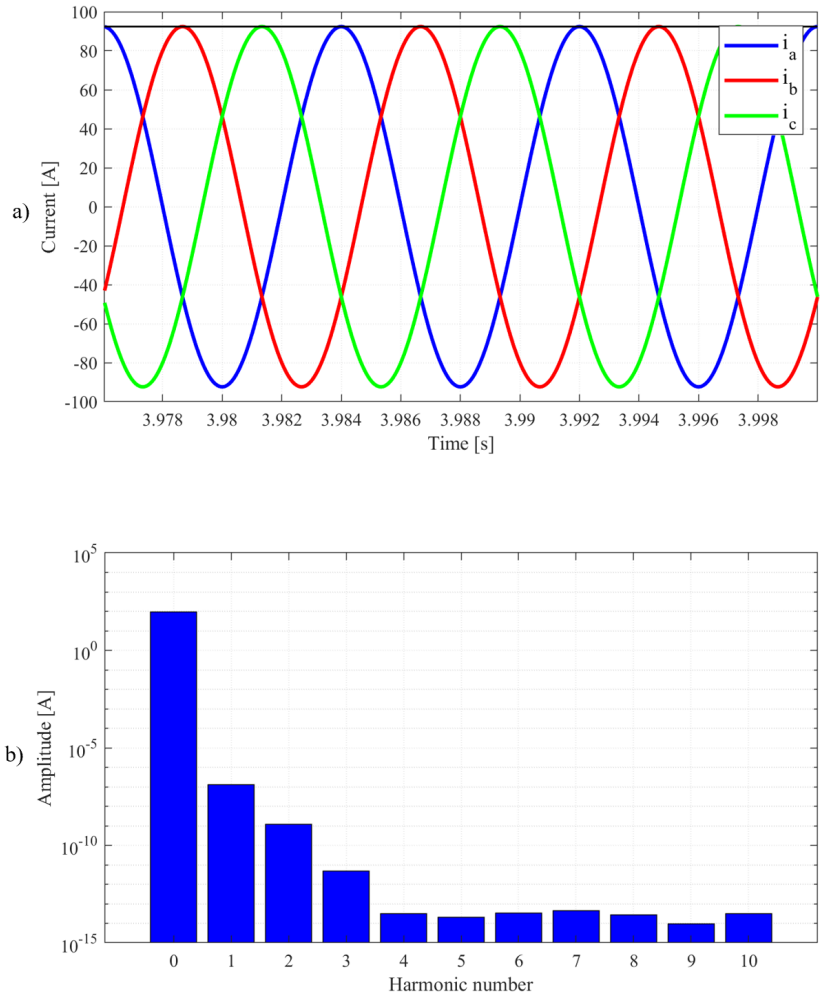

Figure 2.7: PMSM with no fault. Figure a) shows the three phase currents and figure b) show the FFT of the current in the q-axis where the y-axis is a logarithmic scale

In Figure 2.8 a PMSM with a large fault has been simulated. The fault resistance in this case is set to 0.1 Ω and the the affected number of turns is 10 of a total number of 20 turn i.e the phase is 50 % short-circuited. In the figure one can see that the second harmonic is distinctive and much higher than in Figure 2.7. The three-phase currents are also different when a large fault occurs where as the amplitude in the three phases differ form each other. In Figure 2.8 a line have been drawn at the peak of phase a to make it easier to spot the difference.

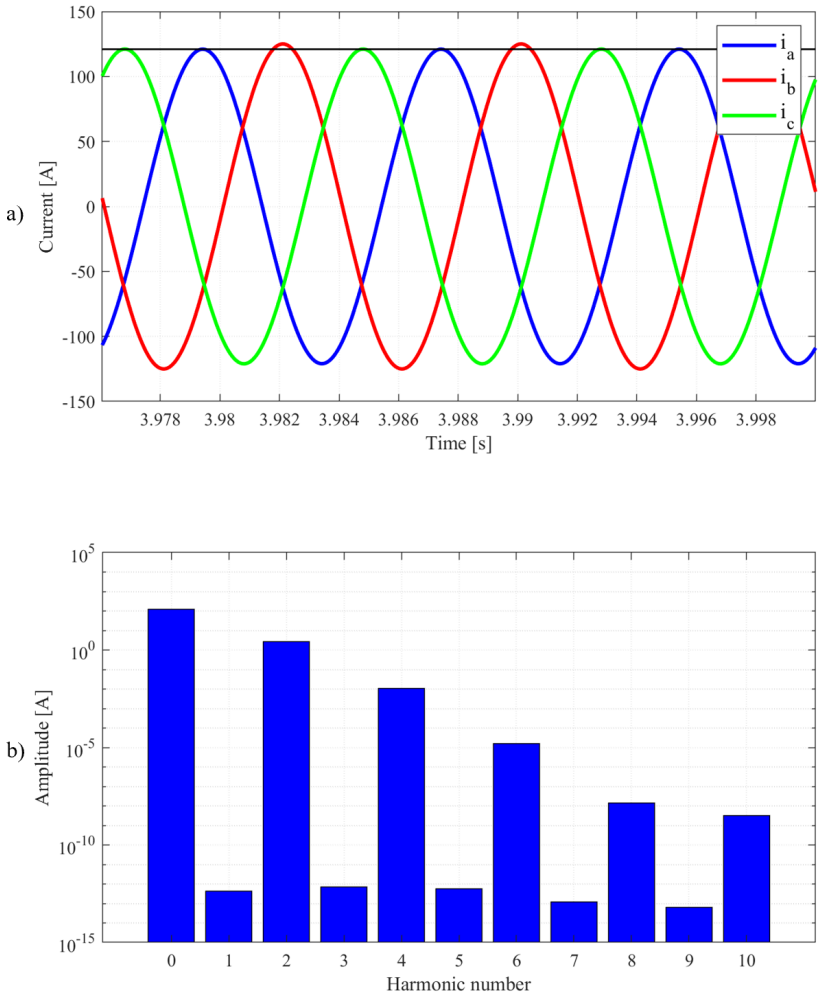

Figure 2.8: Faulted PMSM where μ is set to 50 % and R_f is 0.1 Ω. Figure a shows the three phase currents and figure b show the FFT of the current in the q-axis

Even though a 50 % fault is a large fault it is hard to spot by just looking at the three-phase currents but when one observes the harmonics of the quadrature current of the affected phase it can easily be seen that the second order harmonic stands out. Also worth noting is that since the three-phase currents are unbalanced when a fault occurs the third order harmonic will be prominent in the phase-current harmonic spectrum as shown in Figure 2.9. In the figure the fundamental harmonic is at 125 Hz and then the third order harmonic will be 375 Hz.

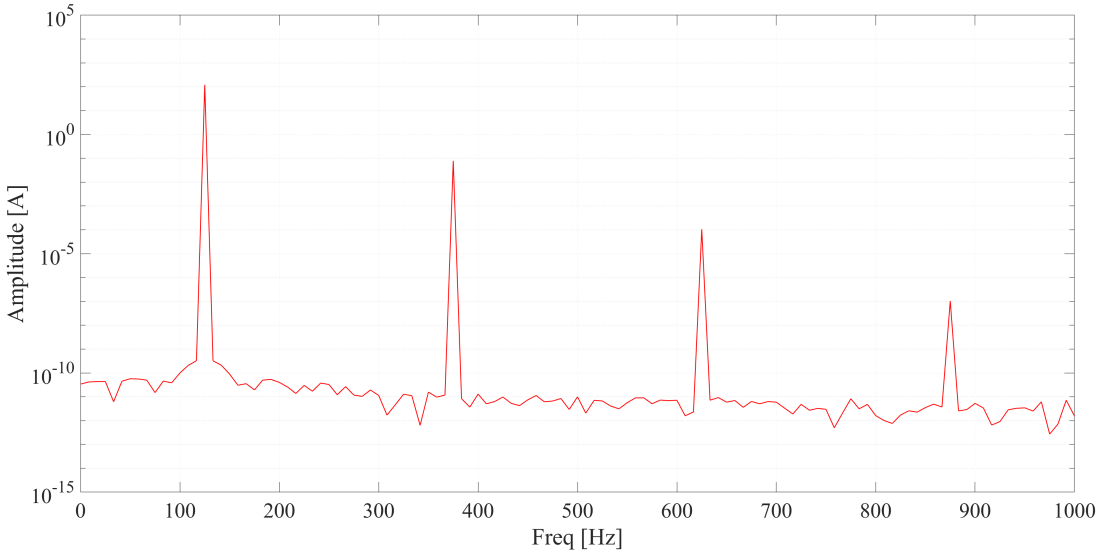

Figure 2.9: Harmonic content of i_a when μ is set to 50 % and R_f is 0.1 Ω

2.3.3 Validation of faulty PMSM model

To validate that the a faulty PMSM is working a PMSM with no fault implemented was modelled and simulated. Using the general PMSM formulas a model of the non-faulty machine has been designed in Matlab and SimuLink. The model with no fault was then used as a benchmark. This benchmark was then compared to the PMSM-model with a fault where R_f was set to a very large value to reduce the fault to a level where it is regarded as a model with no fault. In Figure 2.10 a comparison between these to types of machines has been done. As seen in the figures the faulty machine works as intended.

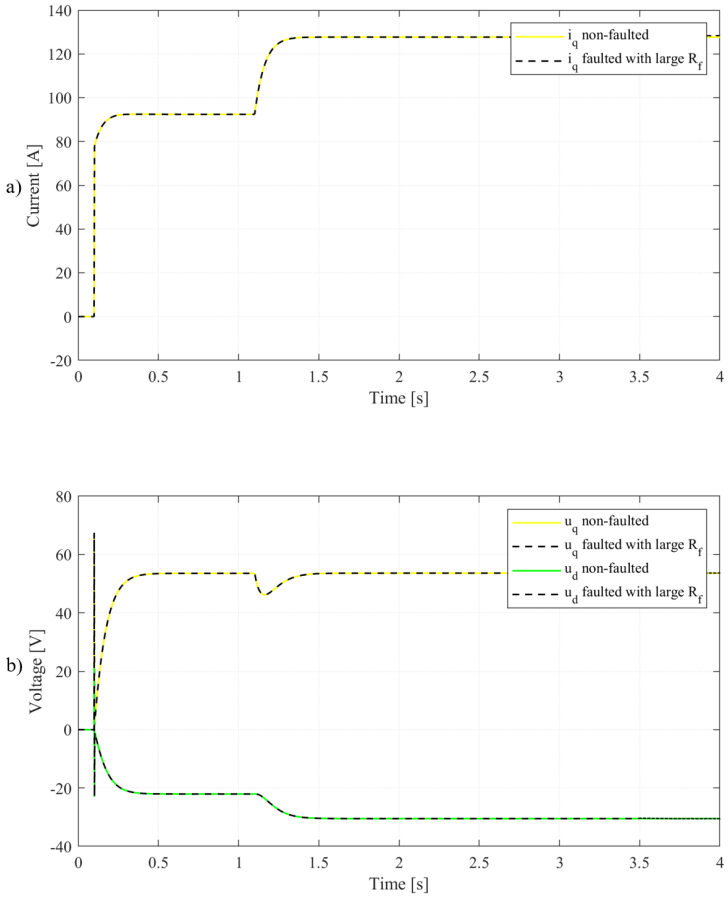

Figure 2.10: Comparison between a PMSM-model without a fault and a PMSM-model with a fault and a very high R_f at the start of the machine with a small load introduced after 1.1 seconds. Figure a) shows the i_q-current and figure b) shows the voltage in dq-component form

3

Fault detection and diagnosis methods

This chapter will firstly present what FDD methods that are considered for the model described in Chapter 2. The most prominent methods depending on their score from Figure 3.1 will be described briefly and discussed. Secondly, the FDD methods that fit the aim of the thesis will be presented in detail and thoroughly discussed.

3.1 Qualitative assessment of FDD methods

This section will describe and explain previous studies in the field. The previous studies will be assigned an description, usually the title of the paper or the FDD method that it mostly resembles. The description of FDD methods will then be divided into different sections depending on the signal primarily analyzed or what umbrella term such as MCSA/MVSA or parameter estimation they are best fitted. The FDD methods will be assigned weights where they are given different points depending on their performance in the papers and further summarised in a final table that can be seen in Figure 3.1. The FDD methods with the highest score in each category section will be briefly explained as well as some perks and shortcomings to see if they are applicable to the aim.

3.1.1 Current and voltage sequence component analysis

The three different sequence components are zero, positive and negative sequence components. The zero sequence components amplitude and phase angle is used to detect fault. It could either analyze the voltage when the motor is wye-connected or the current when the motor is delta-connected. This method is capable of detecting the fault location as well as the fault severity. However, this method needs access to the motors neutral point to measure the voltage which may prove difficult on a live motor [9]. Positive and negative sequence component utilize the relationship of the current and the rotor speed to detect fault. This method is robust against rotor speed changes but has a high sensitivity and might be affected by noise [8].

3.1.2 MCSA/MVSA

The most popular FDD method is the motor current signature analysis (MCSA)[9]. The MCSA is an umbrella term which contains different algorithms such as fast fourier transformation (FFT). An FFT can be done by comparing the harmonics between the measured current from a faulted and a non-faulted PMSM. If the harmonics differ within a previously determined range the method will indicate that a fault has occurred. The kind of MCSA performed in the thesis takes the quadrature current and performs an FFT of said current. The harmonics of the FFT is then extracted and analyzed. As mentioned in Section 2.3.2 the fault is most prominent in the second order harmonic content. But since there is always a second harmonic content the problem is to set a threshold for when a fault should be announced.

3.1.3 Various current and voltage signals

This category is made up by the FDD methods using the output current and voltage but that did not fit the other FDD categories. One of the most prominent FDD method in this category is orthogonal space voltage analysis with FEM [20]. The method uses an FEM to simulate the flux linkage in the machine which is used to calculate the back electromotive force. The purpose of the paper is mainly to categorize the fault severity using the voltage space vector and not detecting the fault. Combined with the use of FEM this method is excluded from possible FDD methods, since is do not meet the aim of the project.

3.1.4 Torque signals

The FDD methods analysing the torque signals are relatively few compared to the other FDD categories in the Figure 3.1. Although, the torque FDD method with continuous wavelet transform (CWT) can assess the number of faulted winding turns, it requires a low pass filter to remove noise. Without the filter the torque signal is considered very sensitive. The method also use machine learning hence it is excluded [26].

3.1.5 Mechanical signals

Finding a fault using a mechanical output such as acoustic noise or vibrations is possible however they do need an additional sensor to be detected. The tests can be done on a live motor but needs to be done in a controlled environment to reduce sounds and other vibrations which could interfere with the fault analysis and is considered a major disadvantage [28].

3.1.6 Parameter estimations

The idea of this FDD method is how the machines different parameters such as flux, impedance, magneto motive force, resistance and inductance behaves and varies during a fault. These methods contains a considerable amount of data and is often the subject of AI technology such as machine learning. Machine learning demands

a high CPU and needs to be applied to each machine separately since the machine data vary from machine to machine. The data also needs to be acquired over time for machine learning to work which can prove to be a bit cumbersome. Another approach is modeling the PMSM as a permeance/reluctance network. This is very similar to how high power systems are analyzed [37]. The major advantage with this method is that it is requiring substantially lower CPU and at the same time provide similar results [37].

3.1.7 Flux signals

The most common FDD method in Figure 3.1 within the flux signal category is the search coil method. This method is not considered since it uses additional hardware in the motor design. Adding a search coil to a motor is not only costly but can affect the performance of the motor. This could be a valid method if implemented when designing and building a new machine [43].

3.1.8 Weights

When ranking the different FDD methods the most significant characteristics has been assigned as weights. The weights, except sensitivity and complexity, has the same weight where they get one point if the answer is yes, minus one point if the answer is no and an unknown weight gives zero points. The sensitivity and complexity can give from one point if the sensitivity/complexity is very low down to minus one point if the sensitivity/complexity is very high, see Figure 3.1. To get an understanding of each weight a short description is presented in this section.

- **Motor :** What type of electrical motor this method is using. PMSM is not only considered since some FDD categories with other motors might have valuable input.
- **Fault identification (FI) :** Whether the FDD method can locate the fault and determine what kind of fault it is. Such as winding fault, coil fault, phase fault or open circuit fault.
- **Online :** If the FDD method can be applied on a live machine or has to be executed on an offline machine.
- **Noninvasive :** There is no need to customize the machine to extract the output signals needed for the FDD method.
- **Sensitivity :** The sensitivity of the output signals. Less sensitive signals are easier to read where sensitive signals are more difficult to read.
- **Fault severity :** If the fault compromise the performance of the machine.
- **Unaffected by other faults and noise (UBOFN) :** If the results from the FDD will be compromised due to other faults and noises.
- **Independent of motor parameter (IOMP) :** If the FDD method can be applied to other motors without changing the parameters of the FDD method.
- **Sensorless :** Whether there is a need for extra sensors or not to extract the signals from the motor.
- **Low CPU :** If the required computing power for the FDD method is low or not.

- **Verified experimentally (VE) :** If the FDD method has been tested on a motor in practice or if the FDD method is tested in a simulation.

- **Complexity :** If the FDD method contains machine learning the complexity will be considered very high. If it contains finite element method (FEM) the complexity will be considered high. If it contains neither the complexity will be regarded as medium.

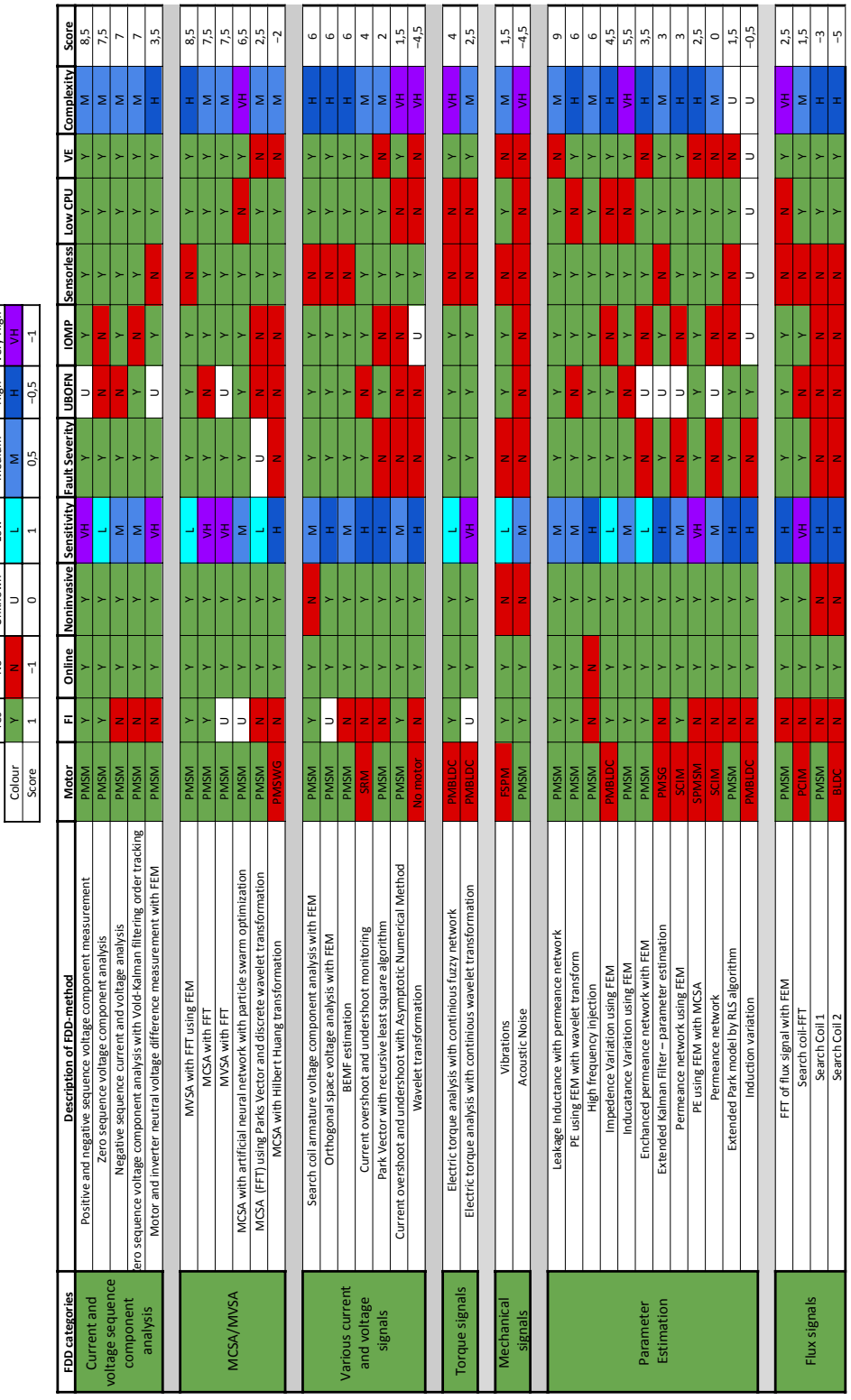

Figure 3.1: Summary of the different FDD methods considered with weights and score specified as well as the score and colour system specified. Reference [8]-[45] from top to bottom

3.2 Permeance network

With a permeance network the flux flowing in the different parts of a PMSM can be estimated. An interesting FDD method would be to analyze the flux when the PMSM is fed with parameters from a healthy motor and compare that flux with the flux from a PMSM with un-healthy parameters. The difference from a finite elemental analysis is that the permeance network requires fewer calculations which in turn requires less CPU. This is especially interesting for the automotive industry where fast calculations are required. In this thesis the permeance network suggested configuration is based on [35],[37] and [39].
Estimating different parameters can be done constructing a state variable model. The model consist of a magnetic equivalent circuit (MEC) where the parameters are derived from geometrical data of the electric machine. One part of the parameters are usually estimated in permeance or reluctance. The second part of the parameters are the magneto motive force (MMF) which are dependent on both the stator windings and the permanent magnets in the rotor. Combining these two parameters you can define the potentials between two nodes as (in this example between the stator tooth and the stator base),

$$M_{st} - M_{sb} = \frac{\phi}{P} + MMF \tag{3.1}$$

where $M_{st,i}$ and $M_{sb,i}$ are the magnetic potential between the stator tooth and the stator base, ϕ is the flux flowing between these potentials, P is the permeance in series between the nodes and MMF is the magneto motive force from either the windings or the magnets.

3.2.1 Node analysis

Both the stator and the rotor will be divided into nodes separately. The nodes are a segment of the stator and rotor and are split where the rotor and the stator repeats itself. The stator repeats itself around the stator slots and the rotor repeats itself around the magnets. The stator node will be expressed as i and take the value from 1 to N_{ss} where N_{ss} is the total number of stator slots in the machine. Likewise, the rotor nodes will be expressed as j and have the value 1 to N_{pp} where N_{pp} is the total number pole-pairs.

3.2.2 Permeance estimations

The equations for permeance estimations is based on the geometry of the machine. Permeance values can be obtained with the formula

$$P = \frac{1}{\Re} = \frac{1}{\int_0^L \frac{dl}{\mu S(l)}} \tag{3.2}$$

Where $\Re$ is reluctance, L is the stack length of the machine, l is the integration variable, S the cross sectional area and μ is the permeability of the material.

In this method most elements can be regarded as rectangular for simplicity purpose. The permeance can then be estimated to be

$$P_{rectangular} = \frac{\mu S}{l} \tag{3.3}$$

The permeances considered in the stator can be the divided into different elements as illustrated in Figure 3.2. The element P_{sb} represent the permeance of the stator base, P_{st} the permeance of the stator tooth and P_{stst}, the stator tooth-tip-to-tooth-tip permeance.

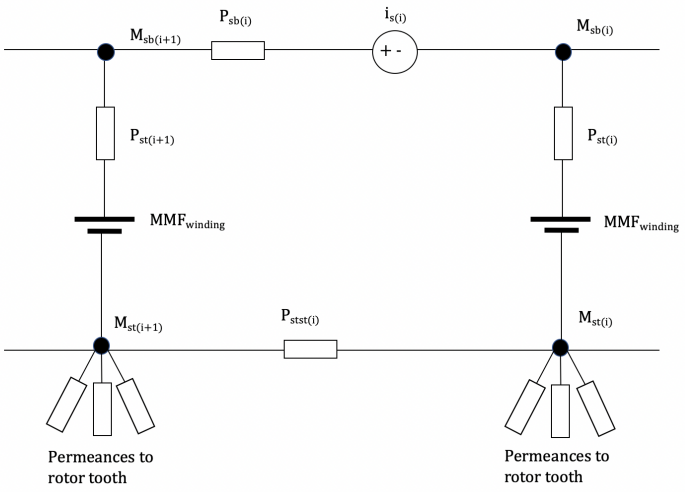

Figure 3.2: Magnetic equivalent circuit of the stator

The permeances in the rotor can be expressed similar to the stator, illustrated in Figure 3.3. Where P_{rb} represent the permeance of the rotor base, P_{rt} the permeance of the rotor tooth, P_{rtrt} the rotor tooth-tip-to-tooth-tip permeance and P_{rtc} the permeance rotor-to-center.

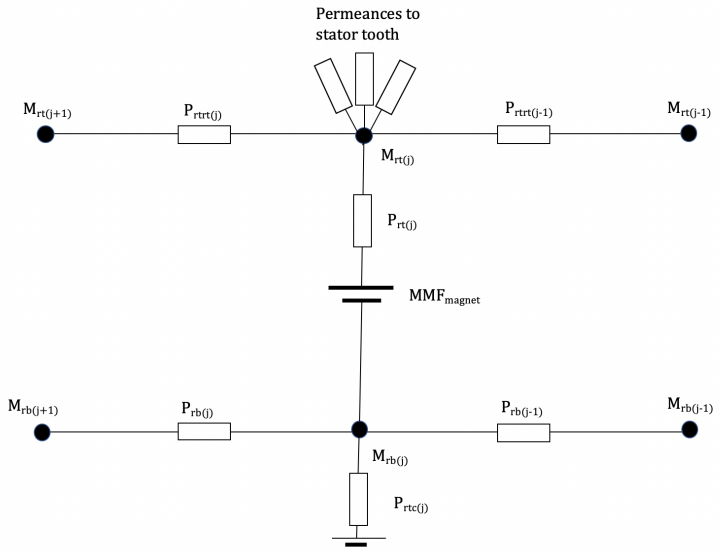

Figure 3.3: Magnetic equivalent circuit of the rotor

Between the stator and rotor is the air-gap. The air-gap permeance value is varying due the rotor position in respect to the stator position. The permeance value is the highest when stator tooth and the rotor tooth is aligned. If a stator tooth and a rotor tooth is not perfectly aligned the permeance decreases until they have no overlap at all and the permeance is zero, as illustrated in Fig 3.4.

Figure 3.4: Air-gap permeance varying with the rotor position in respect to the stator position

3.2.3 Magneto motive force estimations

The MMF is acting like a voltage source in the magnetic equivalent model (MEC), as are shown in Figures 3.2 and 3.3. The MMF can be expressed as

$$MMF = \frac{\phi}{P} \tag{3.4}$$

and is fundamental to the MEC model. The MMF in this model will occur both in the stator due to the windings and the stator current i_s and in the rotor due to the permanent magnets.
The stator windings in a machine can be assumed to have three phases. The windings will be divided into stator nodes. One node contains the windings around one stator slot. The MMF value is dependent on the current going through the winding and the number of turns in the winding. Then the total MMF in each winding becomes

$$MMF_{winding} = \sum N \cdot I \tag{3.5}$$

where N is the number of turns, times the stator current in the coil, I.
The MMF in a magnet can be estimated such as

$$MMF_{magnet} = H_{magnet} \cdot h_c \tag{3.6}$$

where the H_{magnet} is the height of the magnet and h_c is the magnet material coefficient.

3.2.4 MEC-model and node equations

The parameters from the permeance estimation and the MMF from the MMF estimations merge into the equation

$$[P][M] = [\phi_s] \tag{3.7}$$

where the $[P]$ is the permeance matrix containing the permeance in series between the different node combinations. $[M]$ is the the magnetic potentials vector and $[\phi_s]$ is the flux source vector. To obtain $[M]$, the magnetic potential vector can be derived from (3.7) to

$$[M] = \frac{[\phi_s]}{[P]} \tag{3.8}$$

so that the magnetic flux flowing between one node (i) to another node (j) can be estimated with (3.1) and (3.8) as

$$\phi(i,j) = P(i,j) \cdot (M(i) - M(j)) + \phi_s(i,j) \tag{3.9}$$

3.2.5 Solution algorithm

To solve flux equations one has to consider that the flux in a electric machine is not linear. Hence a nonlinear machine needs a nonlinear solution. One proposed solution to the state space equation is the Gauss-Seidel method which is an iterative method. An iterative method is simplified, an algorithm that the first time will guess a solution. Based on the guess of the first solution it will estimate a second solution. It will continue estimating until the difference between the estimations is sufficiently small or number of estimations exceeds a predetermined value.

3.2.6 Summary of permeance network

A PN-network might be used as the base for a FDD method because of the simplicity of the network. To achieve a fully functioning online FDD method the signals from the machine has to be read online as well. To confirm the permeance network it is also recommended to compare it to a FEM. This might be possible to achieve but will be a topic for further studies since.

3.3 Motor current signature analysis using FFT

The MCSA is one of the most popular FDD method [9]. The objective of the method is to detect a fault by measuring the current of the machine and finding anomalies. In this thesis the FDD method using FFT is obtained from [14]. To continuously be able to detect fault on a live PMSM an algorithm is defined as shown in Figure 3.5.
Firstly to extract the harmonics of the q-current the machine must achieve steady state to be able to provide accurate data. A simple function can detect whether the machine has reached steady state, such as

$$|w_r(k) - w_r(k-1)| \leq |0.01 \cdot |w_r(k-1)| \tag{3.10}$$

where $w_r(k)$ is the electrical speed of the PMSM at a given moment in k intervals. This function will see if the speed has changed more than one percent from the previous value in a predetermined time interval. If not, the machine can be considered to be in steady state. The speed $w_r(k)$ is also used to calculate the fundamental frequency.

When the machine is in steady state the q-axis current can be extracted during a number of time periods, in this case 10 time periods is sufficient. Executing an FFT on the q-axis current during said time periods will provide the current harmonics. The second order of the current harmonics is extracted into the variable h_{q2}. A fault index to determine fault is introduced as

$$Fault_{index} = \frac{h_{q2}}{h_{2n}} \tag{3.11}$$

where h_{2n} is the magnitude of the normalized second order harmonic of the q-axis current when the machine is operating under non-fault condition at the same operating point. To obtain h_{2n} a linear interpolation calculation is used as follows

$$h_{2n} = \frac{h_{2b} - h_{2a}}{I_b - I_a}(I_{q_{avg}} - I_a) + h_{2a} \tag{3.12}$$

where h_{2b} is the magnitude of the second order harmonic q-axis current under high load condition and h_{2a} is under low load condition. I_b is the average q-current under high load condition and I_a is under low load. The variables h_{2b}, h_{2a}, I_b and I_a are predetermined from previous simulations with varying load and thus need to be saved prior to the computation of the algorithm. I_{qavg} is the measured average current at the actual operating condition. The linear interpolation calculation provides the means to determine a fault even with varying load. The fault index threshold is set to be 1.5 due to the possibility of noise during measurement. If the signals were ideal the fault threshold could be set to one. In Table 3.1 the values used to calculate the normalized second order harmonic at a speed of 1500 rpm is presented.

Table 3.1: Values used in the MCSA when Ω_r is 1500 rpm

Parameter	**Value**
h_{2a}	145 nA
h_{2b}	237 nA
I_a	92 A
I_b	151 A

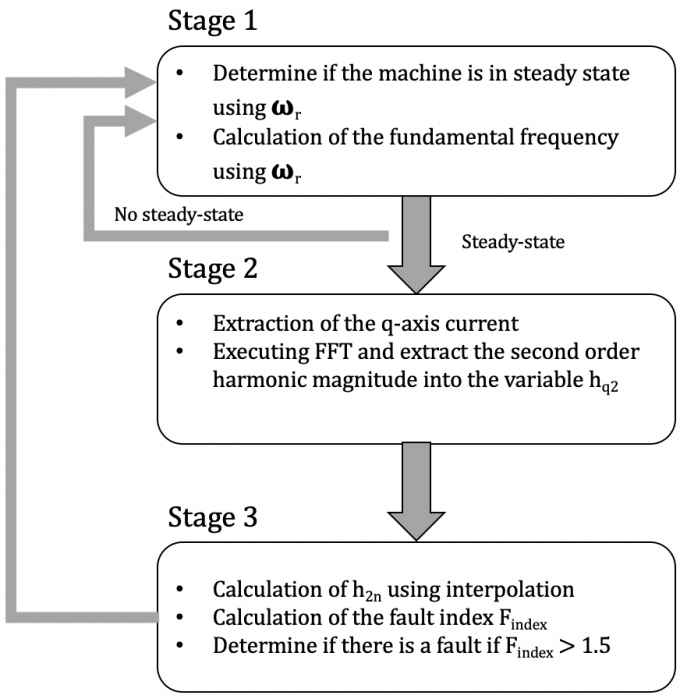

Figure 3.5: Description of the MCSA algorithm using FFT

3.4 Zero sequence voltage component

The FDD method zero sequence voltage component (ZSVC) is considered due to it's high score in Figure 3.1 and since it is applicable to the wye-connected model in Chapter 2. The ZSVC is based on [46], [11] and is using the model from [6]. The ZSVC can be derived from (2.35) as

$$V_0 = \frac{1}{3}(u_a+u_b+u_c)+\frac{1}{3}(e_a+e_b+e_c)-\frac{1}{3}(L_{a2}+M_{a1a2}+M_{a2b}+M_{a2c})\frac{di_f}{dt}-\frac{1}{3}R_{a2}i_f \quad (3.13)$$

where $\frac{1}{3}(e_a+e_b+e_c)$ is the zero sequence back-emf and can be defined as e_0. Due to the the fact that PMSMs are usually fed from a PWM inverter the machine will be injected with a zero sequence voltage. Hence $(u_a+u_b+u_c)$ will not be zero. Adding a resistor network to the circuit as depicted in Figure 3.6 will cancel out the zero sequence voltage injected from the PWM and thus create a neutral point. This will give the equation

$$V_{0,m} = \frac{1}{3}(e_a+e_b+e_c) - \frac{1}{3}(L_{a2}+M_{a1a2}+M_{a2b}+M_{a2c})\frac{di_f}{dt} - \frac{1}{3}R_{a2}i_f \quad (3.14)$$

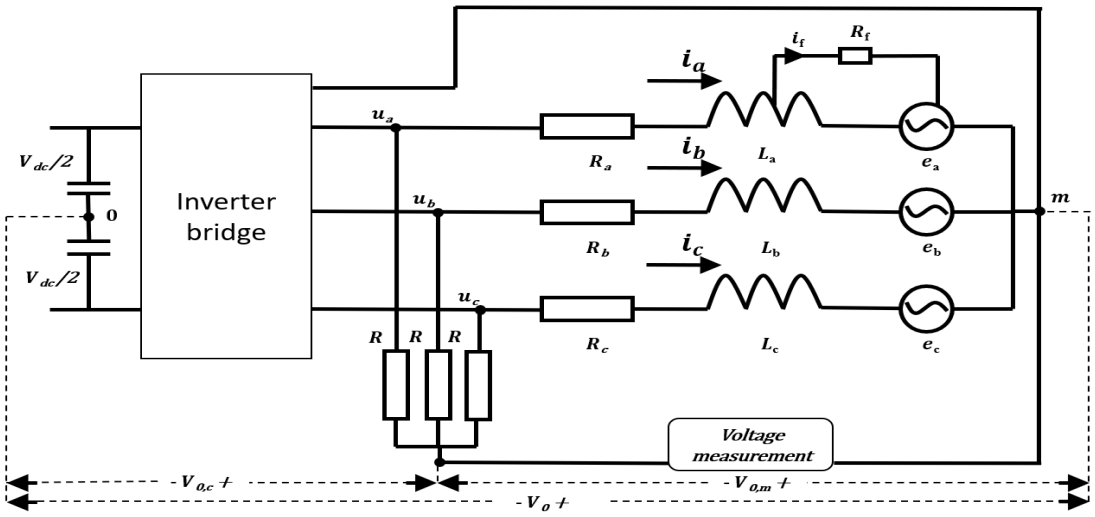

Figure 3.6: Inverter bridge feeding a wye-connected PMSM with fault in phase A. A resistor network is added to the phases to create a neutral point

An FFT will be performed on the ZSVC to detect anomalies in the spectral content. In a completely healthy motor there should be no fault currents which makes i_f equal to zero. Hence the ZSVC $V_{0,m}$ in a healthy motor only consists of the zero sequence back-emf, $\frac{1}{3}(e_a+e_b+e_c)$, and should show in the third harmonic and its odd multiples. Instead, when there is a fault, the fault current i_f is not zero. The fault current should create harmonics in the fundamental components of ZSVC $V_{0,m}$ as well as odd harmonic components. The third order harmonics and its odd multiples should also be present in the fault ZSVC $V_{0,m}$ due to the zero sequence back-emf. According to [46] the amplitudes of the fundamental harmonics differs the most between a PMSM with fault and a healthy PMSM due to an induction phenomenon with the permanent magnets and should be used as a fault indicator.

4

Simulations

In the simulation part of the thesis the results from the FDD-methods will be presented. The FDD-methods will be tested during different fault severity and the sensitivity of the method will be analyzed. In section 2.3.2 two harmonic graphs are presented, one with a very high R_f to simulate a non-faulty machine while still using the model of a faulty machine and one with a severe fault where R_f is 0.1 Ω and μ is 50 %. In Figure 4.1 a comparison between the two harmonic graphs are shown, one with no fault and one with 5 % short circuited turns and $R_f = 0.1\Omega$. It is easily noticed that the even order harmonics are higher in the faulty machine. The greatest one, apart from the fundamental harmonic, is the second order harmonic, which is the one observed when performing the MCSA FDD-method.

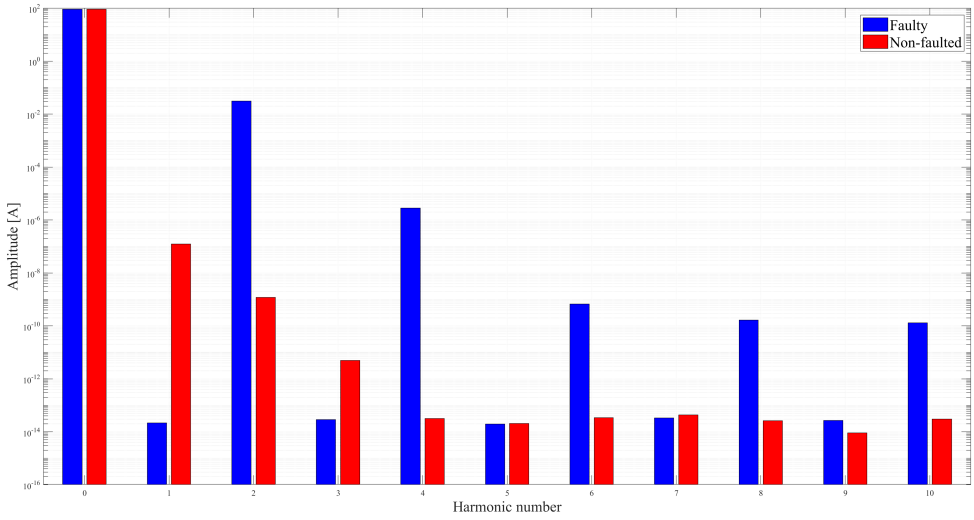

Figure 4.1: comparison between non-faulted harmonics of i_q and with a fault of μ=5 % and $R_f = 0.1$ Ω

In Figure 4.2 the fault resistance, R_f, have been set to decrease linearly and μ is set to 5 %. It can be seen in the graph that the fault resistance is at approximately 27 Ω when the threshold is exceeded. Then the fault index will increase at an exponential rate when the fault resistance decrease further.

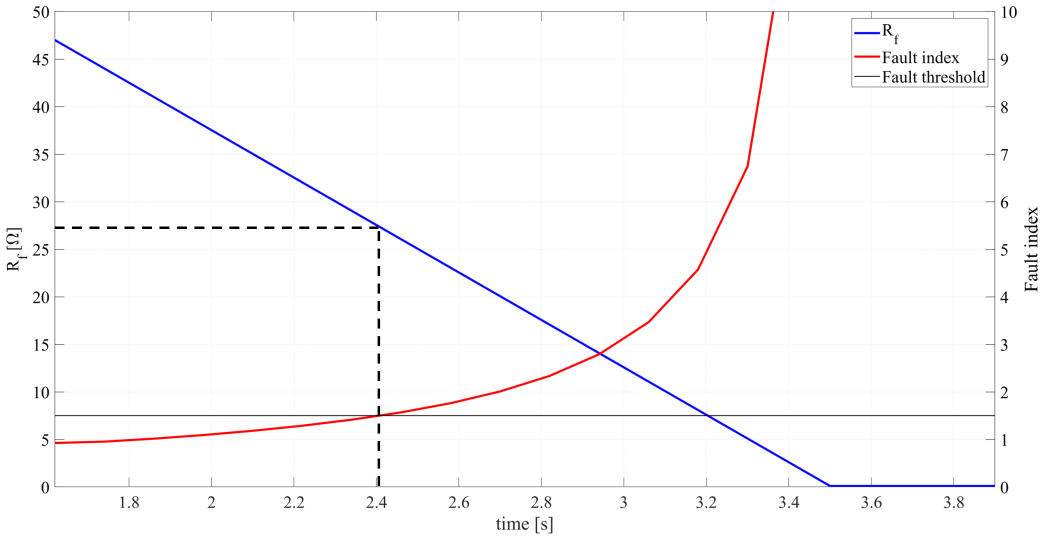

Figure 4.2: The graph shows how the fault index increase when R_f decrease linearly from 50 to 0.1 Ω and μ=5 %

In the case of this thesis a μ of 5 % is the same as a turn-to-turn fault with just one turn short circuited, since $\mu = \frac{N_f}{N_s}$ and the total number of turns is 20. In Figure 4.3 the fault resistance have been decreased linearly from 1000 to 0.1 Ω. Since the duration of the ramp function is the same as in Figure 4.2 the slope will be higher and because of that the lesser faults will quickly change from a low fault index to a big fault index when R_f is getting closer to the fault threshold. Figure 4.3 shows that the difference between a fault with a μ of 5 % and 75 % is very large. In the figure only a μ of 5 %, 10 % and 25 % are under the fault threshold some time during the simulation.

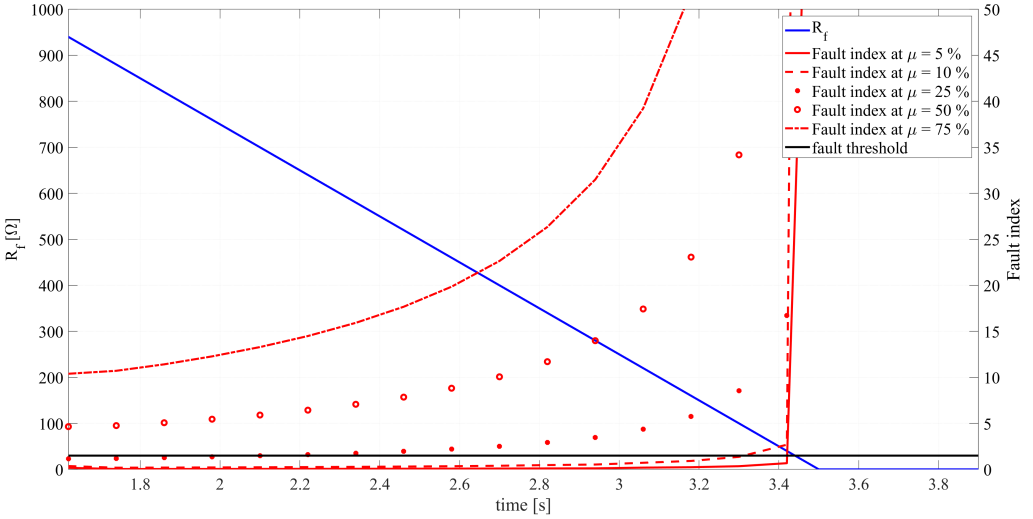

Figure 4.3: The fault index when R_f is decreased from 1000 to 0.1 Ω during different amounts of short-circuited turns

To show at what R_f the threshold at different μ lies two different simulations have

been executed. In Figure 4.4 the threshold of μ at 25 %, 50 % and 75 % are presented. As can be seen in the figure the fault index threshold for these fault occur at a much higher R_f. In the simulation R_f is decreased linearly from 10000 to 100 Ω.

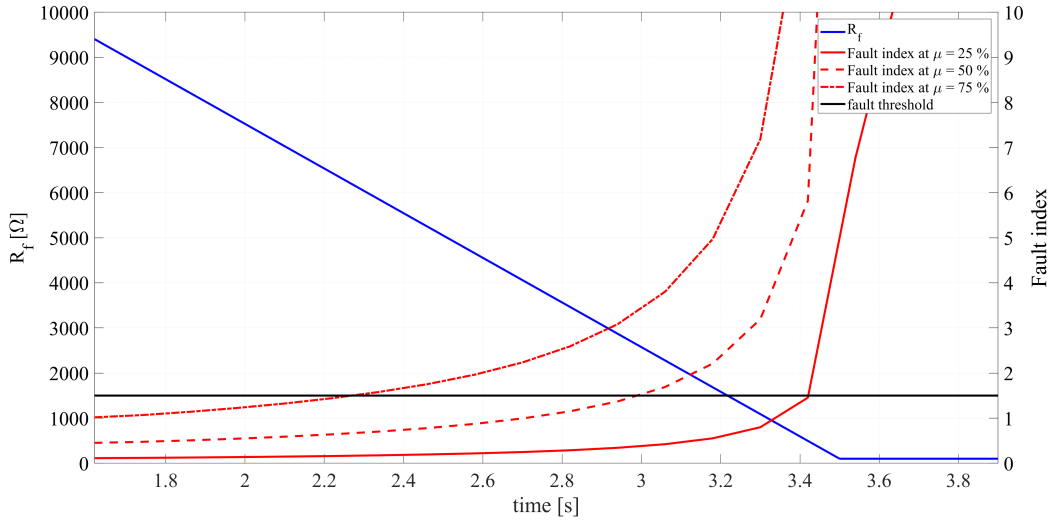

Figure 4.4: The fault index when R_f is decreased from 10000 to 100 Ω during different amounts of short-circuited turns

In Figure 4.5 the fault resistance is decreased linearly from 150 to 0.1 Ω during a one and two short-circuited turns fault.

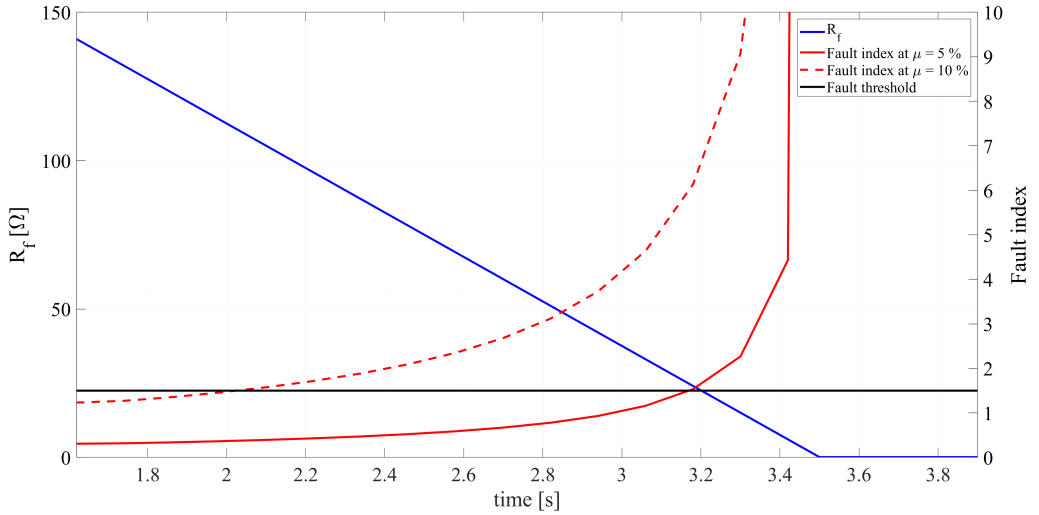

Figure 4.5: The fault index when R_f is decreased from 150 to 0.1 Ω during different amounts of short-circuited turns

The MCSA FDD-method was also simulated during different load conditions. In Table 4.1 fault resistance and fault current at the fault index threshold are presented. Since to acquire a precise FFT several periods, in this case 12, needs to be in each FFT calculation the amount of fault index calculations for a certain amount of time is relatively low. In the case of this thesis the fault index was calculated 20 times during a 2.28 second long simulation. Therefore, the R_f and I_f values are approximations.

Table 4.1: R_f and I_f, when the fault threshold is met, at different amount of extra load torque

$T_{L,extra}$	μ	R_f	I_f
0 Nm	5 %	27 Ω	103 mA
5 Nm	5 %	23 Ω	123 mA
10 Nm	5 %	20 Ω	151 mA
15 Nm	5 %	17 Ω	179 mA
0 Nm	10 %	111 Ω	51 mA
5 Nm	10 %	96 Ω	60 mA
10 Nm	10 %	85 Ω	69 mA
15 Nm	10 %	71 Ω	86 mA
0 Nm	25 %	694 Ω	20 mA
5 Nm	25 %	588 Ω	24 mA
10 Nm	25 %	530 Ω	28 mA
15 Nm	25 %	426 Ω	36 mA
0 Nm	50 %	2628 Ω	11 mA
5 Nm	50 %	2248 Ω	13 mA
10 Nm	50 %	2090 Ω	14 mA
15 Nm	50 %	1689 Ω	18 mA
0 Nm	75 %	6193 Ω	7 mA
5 Nm	75 %	5255 Ω	8 mA
10 Nm	75 %	4601 Ω	9 mA
15 Nm	75 %	3948 Ω	12 mA

As it can be seen in the table a higher load will make the FDD detect a fault later, at a lower fault resistance, than with a lower load. This is because the current in the machine is higher when a higher load is applied and a higher current leads to a lower resistance. In Figure 4.6 the first part of Table 2.1, 5 % short-circuit, is presented. It can be seen in the figure that a higher load gives a lower R_f at the threshold. It can also be seen in Table 4.1 that a higher amount of short circuited turns gives a lower fault current when the threshold is met. This is because a higher μ will make the three phase current become more unbalanced which will lead to a higher i_q second order harmonic and therefore detect the fault at a lower fault current.

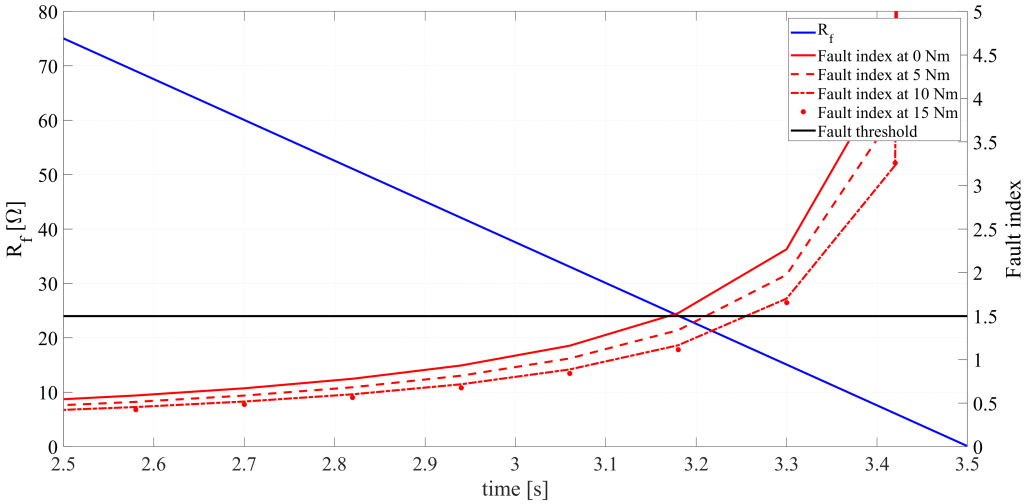

Figure 4.6: The fault index when R_f is decreased from 150 to 0.1 Ω during different load conditions at 5 % short-circuit

A ZSVC has also been implemented to detect the fault. As can be seen in Figure 4.7 the fundamental component of the zero sequence voltage is very close to zero when no fault is present. But when adding a small fault the fundamental component is much higher, but still relatively low, at around 1 mV.

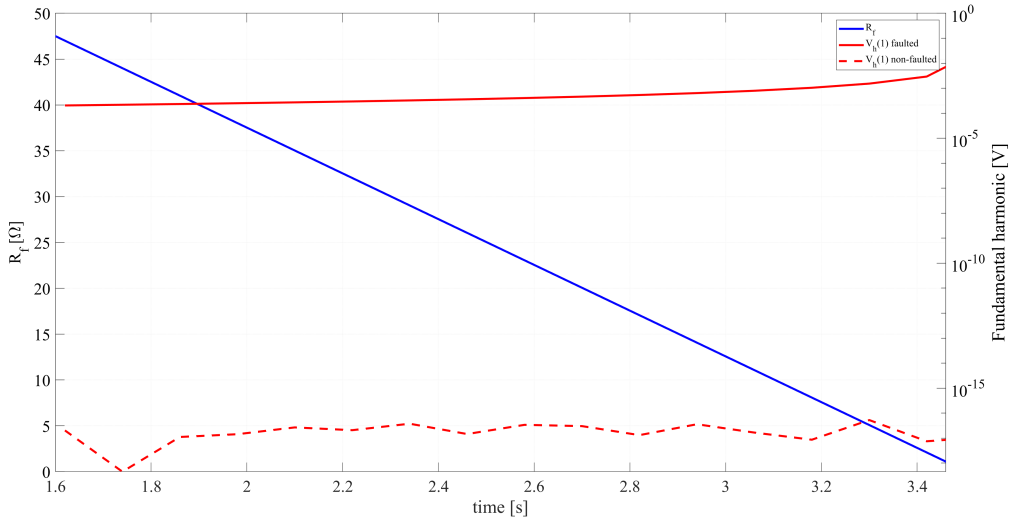

Figure 4.7: Non-faulted zero sequence voltage fundamental harmonic and faulted zero sequence fundamental harmonic when R_f is decreased from 50 to 0.1 Ω at 5 % short-circuit

In Figure 4.8 the harmonics of the zero sequence voltage during no fault and a small fault can be seen. The fault has one short circuited turn and a fault resistance of 0.1 Ω. It can be seen in the graph that a small fault impacts the harmonics very much. It can be seen that the fundamental component is the most significant. The third order harmonic and its multiples are also visibly larger than the rest.

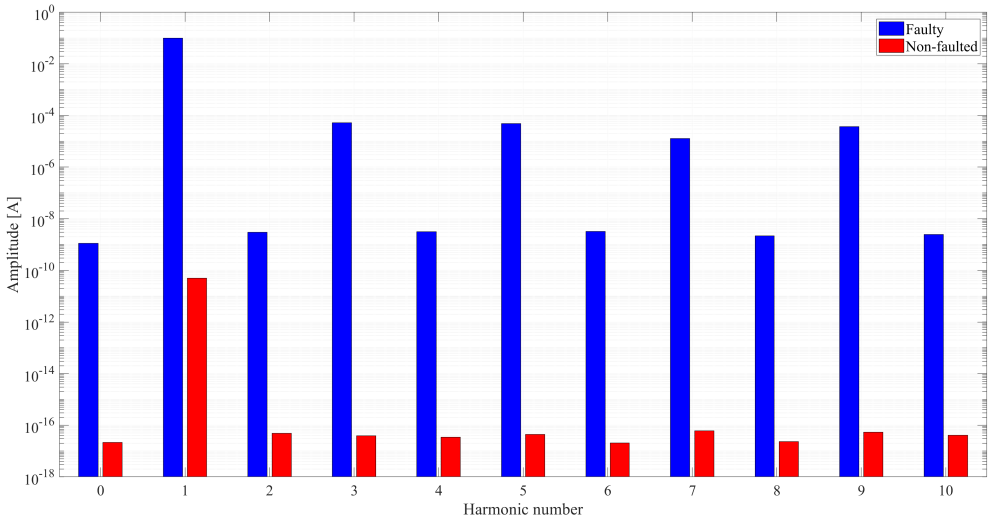

Figure 4.8: ZSVC FFT when no fault and at a short circuit of $\mu = 5$ % and $R_f = 0.1$ Ω

In Figure 4.9 a bigger fault has been simulated. The fault has two short circuited turns and a fault resistance of 0.1 Ω. The bigger fault gives a small increase in the fundamental component compared to the previous fault severity.

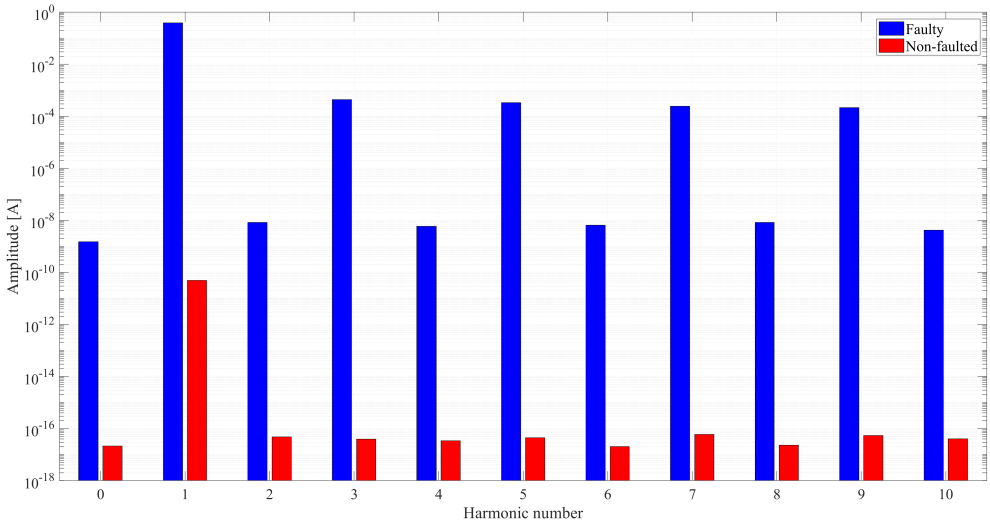

Figure 4.9: ZSVC FFT when no fault and at a short circuit of $\mu = 10$ % and $R_f = 0.1$ Ω

5
Discussion

In this chapter the different parts of the thesis will be discussed. It is divided into the main parts of the whole thesis.

5.1 Modelling of PMSM

The faulty PMSM model used in this thesis is validated by comparing it to a PMSM model without any fault. This is shown in Figure 2.10. Since the PMSM is completely ideal no harmonics is visible in the non-faulted machine. However, in the faulted machine all harmonics are noticeable even when R_f is very high, as to simulate a non-faulted machine with a faulty model. When a fault is introduced, by setting a low R_f, the second order harmonic of the quadrature current is expected to be prominent, which as been confirmed in Figure 2.8 [14]. Since the three-phase current is unbalanced, as shown in Figure 2.8, the third order harmonic is larger in the three-phase currents. This is then multiplied by the fundamental harmonic when transformed into a synchronous reference frame which is why the second order harmonic is larger in the quadrature current. This is the proven accurate by the results acquired in the thesis.
Even though the PMSM model is validated it could be improved on by conducting a FEM on the machine to get more precise inductances. In this thesis the inductances was instead calculated by using equations from [6] which is proven to be within accepted error margins. Since all the necessary parameters needed to calculate the inductances were not available for the machine used, a reference PMSM was used as well. It was deemed reasonable to scale the inductances from the reference PMSM to the actual PMSM since the geometry of the two machines are similar.

5.2 Fault detection and diagnosis

The FDD method with the highest score is the permeance network. The permeance network offer similar measurements as the FEM but requires less computing power. The FEM is widely used when designing the motor but is limited due to high CPU and is not deemed suitable for an FDD purpose in the automotive industry. The main reason why the permeance network is not carried out is that to verify that the permeance network works as intended it needs to be confirmed with the FEM. To design a motor in FEM more parameters then provided is needed and thus the permeance network could not properly be validated.

The FDD methods chosen, the MCSA with FFT and ZSVC, is not the FDD methods with the highest score. However, the MCSA does offer some advantages in term of implementation on a real motor compared to the other methods. By just measuring the current and the electrical rotor speed of the PMSM, perform a few measurements and calculations and an accurate fault detection can be accomplished. The computing power needed to perform the method is relatively low compared to the other methods which give it advantage especially in the automotive industry where fast calculations are needed.
It should first and foremost be noted that the MCSA with FFT was implemented on a ideal PMSM. This will affect how the sensitivity of the method is analyzed. Since no noise is implemented in the PMSM model the sensitivity can not accurately be determined. This could be accomplished by doing a physical experiment or by implementing noise in the simulation. In the simulations that have been conducted it can be observed that the method is working and can detect a small fault at an early stage, at an R_f of about 27 Ω. It can be confirmed, that this is an early stage detection in the papers [6],[47] and [7] where an R_f of 10 Ω or lower is considered a fault. It can also be observed that an higher torque load will lead to that the fault is detected at a lower R_f. The variable R_f is a representation of the insulation strength between the windings. R_f can change over time due to wear of the insulation but should be considered a constant resistance in the simulation process. If R_f is considered to be constant the conclusion is that the fault will be detected at a later stage, at a higher I_f, with higher torque load. Hence the FDD method detects a fault later at a higher torque load compared to a low torque.
Since the ZSVC has no fault threshold determined in [46] it is hard to set a threshold with no physical experiments. It can be determined that the ZSVC is a lot more sensitive than the MCSA and should therefore have a higher threshold since noise will possibly affect the method more. The difference in the fundamental component is so large that a threshold could be set to the non-faulted fundamental component times 10 and then detect a fault earlier than the MCSA. However it could also be harder to detect the fault since the voltage amplitudes when a fault occurs is still very low and a small anomaly could be seen as a faulty machine. One way to solve this is to measure the zero sequence voltage for some period of time and if the voltage is higher than a predetermined value during this whole period a fault can be determined. The ZSVC also needs extra equipment to work which could be hard to execute with a machine in a vehicle and would also make the method more expansive compared to the MCSA.

5.3 Sustainability

One of the most urgent and important problem of today might be the sustainable question. More companies start to prioritize sustainability and some even prioritize it before maximum profit [48]. Earth's resources are limited and should be treated as such. Society's awareness of sustainability is increasing and the norm is to include it in business plans, annual meeting of shareholders and scientific papers.
Sustainability is not just about the ecological aspect but covers the social and even the economical aspect. In this paper the sustainable aspect of improving the PMSM

and prevent it from failing will be discussed. Considering that the lifetime span of the PMSM will increase as well as the operating security.

5.3.1 Social aspect

The transportation section is shifting from the fossil fuel towards renewable fuels including electrification which includes the PMSM. Public transport with electric engines such as trains, cars and buses would be more viable since the life span of the motor could increase. This also means that the use of the combustion engine would decrease since it is a shared market. That would decrease problem such as smog in bigger city's. Smog is a major health problem today and is considered a danger to the general population [49].
To manufacture a PMSM you need rare earth minerals and magnets which usually mined in underdeveloped countries. The working conditions in the mining industry in these countries are substandard to say the least and a increase of this industry could lead to more human suffering [50].
The aim of the thesis is to detect a stator winding fault in a PMSM at an early stage thus preventing it from failing. In an automotive perspective this is of the utmost importance to ensure personal safety. Hence, a FDD method will increase the safety of road users.

5.3.2 Economical aspect

The investment cost of an electric vehicle today is usually higher than the standard combustion vehicle. Today the economical argument for buying a electric vehicle is that the fuel cost less or governmental subsidies. With a safer operation and longer lifetime of the vehicle, the maintenance would decrease and hence the total cost.
A more reliable and safer PMSM could also change the electricity market. If electric transportation become the leading form of transportation the demand for electricity would increase.

5.3.3 Ecological aspect

With PMSM:s need for rare earth minerals such as permanent magnets the mining of these minerals are more profitable. The mines that are created and existent affect the natural landscape. The mines pollute the ground water and are affecting the bio diversity in a negative aspect [50].
The use of PMSM is also connected with the use of batteries. Batteries is also dependent on the mining industry which enhances the negative effect on the environment.
This project aims to increase the lifetime of the PMSM which may reduce the mentioned environmental impact. It could also increase this impacts due to the PMSM being a more profitable choice.
The PMSM is dependent on electric energy which usually is produced by renewable energy sources. Renewable energy sources such as wind-power, solar-power tidal-power and hydro-power has a significant lesser emission of the greenhouse gas CO_2.

Greenhouse gasses increase the greenhouse affect which is slowly and steadily increasing the earths average temperature. With a increased temperature the arctic poles will melt and raise the water level and decrease the area of livable land. Cities close to the sea will need a comprehensive infrastructure to sustain. This might be possible for developed countries but might prove difficult under developed countries. A higher temperature also increase the extreme weather such as tempest, hurricanes and draught. Once again developed countries might be able to sustain in these conditions but under developed countries might not [51].

6
Conclusion

The aim of this thesis has been to detect a stator winding fault in a PMSM at an early stage. From the simulations it can be seen that the MCSA with FFT detects the fault at an early stage. When there is no extra load the MCSA will detect a small fault, one turn short circuited, when R_f is 27 Ω. It can also be seen that a higher load torque causes it to detect the fault at a higher fault current, for example at an extra load of 15 Nm a fault with one turn short circuited is detected when R_f is 17 Ω which yields a higher fault current of 179 mA compared to the same fault with no extra load at 103 mA. This means that the fault could do more damage before being detected when the machine is operating at a higher load.
Another FDD, the ZSVC, was implemented and proved to also be able to detect the fault at an early stage but since the voltage in the zero sequence is very low the method is a lot more sensitive to noise. To compare it with the MCSA, at one turn short circuited, a fault resistance of 27 Ω and no extra load the zero sequence voltage is 0.4 mV and with a fault resistance of 17 Ω and 15 Nm extra load the zero sequence voltage is 0.6 mV. The fact that it is sensitive, needs access to the neutral point and an instrument that can detect the small voltages makes it a more expensive and less attractive FDD method compared to the MCSA.
To be able to test the FDD methods a PMSM with a fault has been modeled. The model has been verified by comparing it to a non-faulty PMSM and it was concluded that it worked as intended.
To decide what FDD method to develop a number of different FDD methods has been considered. Considering the limitations, the FDD method most suited to meet the aim was the MCSA with FTT. Other FDD methods was described and their working principals has been explained. The best rated FDD method, flux-estimation with permeance network, should be considered in further works since it shows a lot of promise and does not require high computing power. It is also concluded that most of the FDD methods with a high score in the qualitative assessment uses FEM or machine learning and these methods require a higher CPU which would be best for an application when the machine data could be rendered by a powerful CPU which most cars do not have.
To conclude, the aim of the thesis was met, which was to design an FDD method that could detect a fault at an early stage, within the limitations of the thesis.

7
Further work

For further work the parameters for the PMSM should be acquired by doing an FEM or conduct measurements on a real machine to get more precise values. The PMSM could be simulated with added noise to verify if the FDD method could still find the fault at non-ideal conditions since that would more accurately represent a real machine. The FDD method should be tested on a real machine since the analytically modeled machine have estimated parameters and ideal conditions. This would be the most accurate way to validate the FDD method. The FDD method should lastly be implemented on a live machine to test if it works as intended. Ideally all the FDD methods mentioned in 3.1 should be investigated in more detail to have a more fair representation than the weight system. The permeance network could be an interesting base for a FFD method and is suggested for further work.

Bibliography

[1] M. J. Melfi, S. Evon and R. McElveen, "Induction versus permanent magnet motors," Industry Applications Magazine, IEEE, vol. 15, no. 6, pp. 28 - 35, 2009.

[2] C. Gerada, K. Bradley and M. Summer, "Winding turn-to-turn faults in permanent magnet synchronous machine drives," Fourtieth IAS Annual Meeting. Conference Record of the 2005 Industry Applications Conference, 2005., Kowloon, Hong Kong, 2005, pp. 1029-1036 Vol. 2. [Online] Available :https://ieeexplore.ieee.org/stamp/stamp.jsp?tp=arnumber=1518481isnumber=32506, Accessed on: 2019-12-03

[3] Juan C. Quiroz, Norman Mariun, Mohammad Rezazadeh Mehrjou, Mahdi Izadi, Norhisam Misron, Mohd Amran Mohd Radzi, "Fault detection of broken rotor bar in LS-PMSM using random forests," Measurement, Volume 116, 2018. [Online] Available :http://www.sciencedirect.com/science/article/pii/S0263224117307066, Accessed on: 2019-12-03

[4] Bonnett A.H., Yung C. "Increased efficiency versus increased reliability" IEEE Ind. Appl. Mag., 14 (1) (2008), pp. 29-36

[5] L. Harnefors, *Control of Variable-Speed Drives*. 2002

[6] B. Vaseghi, N. Takorabet, F. Meibody-Tabar, A. Djerdir, J. Farooq, and A. Miraoui, "Modeling and characterizing the inter-turn short circuit fault in PMSM", *Electric Machines Drives Conference (IEMDC)*, 2011 IEEE International, 2011, pp. 551-556

[7] J. Härsjö, *Modeling and Analysis of PMSM with Turn-To-Turn Fault*. 2016

[8] Meinguet, F., Semail, E., Kestelyn, X., et al.: "Change-detection algorithm for short-circuit fault detection in closed-loop AC drives", IET Electr. Power Appl., 2014, 8, (5), pp. 165–177. [Online] Available :https://ieeexplore.ieee.org/stamp/stamp.jsp?tp=arnumber=6815119, Accessed on: 2019-12-03

[9] Hang, J., Zhang, J., Cheng, M., et al.: "Online inter-turn fault diagnosis of permanent magnet synchronous machine using zero sequence components", IEEE Trans. Power Electron., 2015, 30, (12), pp. 6731–6741. [Online] Available :https://ieeexplore-ieee-org.proxy.lib.chalmers.se/stamp/stamp.jsp?tp=arnumber=7004080, Accessed on: 2019-12-03

[10] K. Kim, "Simple Online Fault Detecting Scheme for Short-Circuited Turn in a PMSM Through Current Harmonic Monitoring," in IEEE Transactions on Industrial Electronics, vol. 58, no. 6, pp. 2565-2568, June 2011. [Online] Available :https://ieeexplore.ieee.org/stamp/stamp.jsp?tp=arnumber=7869286, Accessed on: 2019-12-03

[11] Urresty, R.J., Romeral, L.: 'Diagnosis of inter turn faults in PMSMs operating under non-stationary conditions by applying order tracking filtering', IEEE Trans. Power Electron., 2013, 28, (1), pp. 507–515. [Online] Available :https://ieeexplore.ieee.org/stamp/stamp.jsp?tp=arnumber=6198360, Accessed on: 2019-12-03

[12] van der Geesi, M., Polinder, H., Abraham, J., et al.: 'Analysis and neutral voltage based detection of interturn faults in high-speed permanent-magnet machines with parallel strands', IEEE Trans. Ind. Electron., 2015, 62, (6), pp. 3862–3873. [Online] Available :https://ieeexplore.ieee.org/stamp/stamp.jsp?arnumber=7039201, Accessed on: 2019-12-03

[13] Immovilli Bianchini, F.C., Lorenzani, E., et al.: 'Evaluation of combined reference frame transformation for interturn fault detection in permanent-magnet multiphase ma-

chines', IEEE Trans. Ind. Electron., 2015, 62, (3), pp. 1912–1920. [Online] Available :https://ieeexplore.ieee.org/stamp/stamp.jsp?tp=arnumber=6880394, Accessed on: 2019-12-03

[14] Kim, K.H.: 'Simple online fault detecting scheme for short-circuited turn in a PMSM through current harmonic monitoring', IEEE Trans. Ind. Electron., 2011, 58, (6), pp. 2565–2568. [Online] Available :https://ieeexplore.ieee.org/stamp/stamp.jsp?tp=arnumber=5518423, Accessed on: 2019-12-03

[15] Boileau, T., Leboeuf, N., Nahid-Mobarakeh, B., et al.: 'Synchronous demodulation of control voltages for stator interturn fault detection in PMSM', IEEE Trans. Power Electron., 2013, 28, (12), pp. 5647–5654. [Online] Available :https://ieeexplore.ieee.org/stamp/stamp.jsp?tp=arnumber=6484985, Accessed on: 2019-12-03

[16] Nyanteh, Y., Edrington, C., Srivastava, S., et al.: 'Application of artificial intelligence to real-time fault detection in permanent-magnet synchronous machines', IEEE Trans. Ind. Appl., 2013, 49, (3), pp. 1205–1214 [Online] Available :https://ieeexplore.ieee.org/stamp/stamp.jsp?tp=arnumber=6480827, Accessed on: 2019-12-03

[17] Hang, J.; Zhang, J.; Cheng, M.; Wang, Z. Fault diagnosis of mechanical unbalance for permanent magnet synchronous motor drive system under non-stationary condition. In Proceedings of the 2013 IEEE Energy [Online] Available :https://ieeexplore.ieee.org/stamp/stamp.jsp?tp=arnumber=4344874, Accessed on: 2019-12-03

[18] C. Wang, X. Liu and Z. Chen, "Incipient Stator Insulation Fault Detection of Permanent Magnet Synchronous Wind Generators Based on Hilbert–Huang Transformation," in IEEE Transactions on Magnetics, vol. 50, no. 11, pp. 1-4, Nov. 2014, Art no. 8206504.[Online] Available :https://ieeexplore.ieee.org/stamp/stamp.jsp?tp=arnumber=6971684, Accessed on: 2019-12-03

[19] Da, Y., Shi, X., Krishnamurthy, M.: 'A new approach to fault diagnostics for permanent magnet synchronous machines using electromagnetic signature analysis', IEEE Trans. Power Electron., 2013, 28, (8), pp. 4104–4112[Online] Available :https://ieeexplore.ieee.org/stamp/stamp.jsp?arnumber=6355697, Accessed on: 2019-12-03

[20] Bianchini, C., Fornasiero, E., Matzen, T.N., et al.: 'Fault detection of a five-phase permanent-magnet machine'. Proc. 34th IEEE IECON, 10–13 November 2008, pp. 1200–1205 [Online] Available :https://ieeexplore.ieee.org/stamp/stamp.jsp?tp=arnumber=4758125, Accessed on: 2019-12-03

[21] Sarikhani, A., Mohammed, O.A.: 'Inter-turn fault detection in PM synchronous machines by physics-based back electromotive force estimation', IEEE Trans. Ind. Electron., 2013, 60, (8), pp. 3472–3484 [Online] Available :https://ieeexplore.ieee.org/stamp/stamp.jsp?tp=arnumber=6339056, Accessed on: 2019-12-03

[22] J. A. Haylock, B. C. Mecrow, A. G. Jack and D. J. Atkinson, "Operation of fault tolerant machines with winding failures," 1997 IEEE International Electric Machines and Drives Conference Record, Milwaukee, WI, USA, 1997, pp. MC3/10.1-MC3/10.3 [Online] Available :, Accessed on: 2019-12-03

[23] M. Khov, J. Regnier and J. Faucher, "Detection of turn short-circuit faults in stator of PMSM by on-line parameter estimation," 2008 International Symposium on Power Electronics, Electrical Drives, Automation and Motion, Ischia, 2008, pp. 161-166 [Online] Available :https://ieeexplore.ieee.org/stamp/stamp.jsp?tp=arnumber=4581092isnumber=4581062, Accessed on: 2019-12-03

[24] W. G. Zanardelli, E. G. Strangas and S. Aviyente, "Identification of Intermittent Electrical and Mechanical Faults in Permanent-Magnet AC Drives Based on Time–Frequency Analysis," in IEEE Transactions on Industry Applications, vol. 43, no. 4, pp. 971-980, July-aug. 2007. [Online] Available :https://ieeexplore.ieee.org/stamp/stamp.jsp?tp=arnumber=4276870, Accessed on: 2019-12-03

[25] Z. Luo and L. Liu, "Adaptive Selection of Wavelet Basis Based on Genetic Algorithm and Its Application," Third International Conference on Nat-

ural Computation (ICNC 2007), Haikou, 2007, pp. 405-409.[Online] Available :https://ieeexplore.ieee.org/stamp/stamp.jsp?tp=arnumber=4344874, Accessed on: 2019-12-03

[26] Awadallah, M.A., Morcos, M.M., Gopalakrishnan, S., et al.: 'A neuro-fuzzy approach to automatic diagnosis and location of stator inter-turn faults in CSI-fed PM brushless dc motors', IEEE Trans. Energy Convers., 2005, 20, (2), pp. 253–259. [Online] Available :https://ieeexplore.ieee.org/stamp/stamp.jsp?tp=arnumber=1432835, Accessed on: 2019-12-03

[27] Awadallah, M.A., Morcos, M.M., Gopalakrishnan, S., et al.: 'Detection of stator short circuits in VSI-fed brushless dc motors using wavelet transform', IEEE Trans. Energy Convers., 2006, 21, (1), pp. 1–8[Online] Available :https://ieeexplore.ieee.org/stamp/stamp.jsp?tp=arnumber=1597314, Accessed on: 2019-12-03

[28] Ojeda, J.; Boisson, J.; Gabsi, M. 5-phase flux switching machine insulation failure detection using vibration monitoring. In Proceedings of the 2014 17th International Conference on Electrical Machines and Systems (ICEMS), Hangzhou, China, 22–25 October 2014; pp. 1039–1043. [Online] Available :https://ieeexplore.ieee.org/stamp/stamp.jsp?tp=arnumber=7013622, Accessed on: 2019-12-03

[29] G. Salim, B. Ouadie and H. Ghaleb, "Vibro-acoustic fault detection and diagnosis in hybrid electric vehicle," 4th International Conference on Power Engineering, Energy and Electrical Drives, Istanbul, 2013, pp. 309-313. [Online] Available :https://ieeexplore.ieee.org/stamp/stamp.jsp?tp=arnumber=6635625, Accessed on: 2019-12-03

[30] N. Leboeuf, T. Boileau, B. Nahid-Mobarakeh, N. Takorabet, F. Meibody-Tabar and G. Clerc, "Inductance Calculations in Permanent-Magnet Motors Under Fault Conditions," in IEEE Transactions on Magnetics, vol. 48, no. 10, pp. 2605-2616, Oct. 2012 [Online] Available :https://ieeexplore.ieee.org/stamp/stamp.jsp?tp=arnumber=6193436, Accessed on: 2019-12-03

[31] O. A. Mohammed, S. Liu and Z. Liu, "Internal Short Circuit Fault Diagnosis for PM Machines Using FE-based Phase Variable Model and Wavelet Analysis," 2006 12th Biennial IEEE Conference on Electromagnetic Field Computation, Miami, FL, 2006, pp. 157-157. [Online] Available :https://ieeexplore.ieee.org/stamp/stamp.jsp?tp=arnumber=4137782, Accessed on: 2019-12-03

[32] J. Arellano-Padilla, M. Sumner and C. Gerada, "Winding condition monitoring schemefor a permanent magnet machine using high-frequency injection," in IET Electric Power Applications, vol. 5, no. 1, pp. 89-99, January 2011. [Online] Available :https://ieeexplore.ieee.org/stamp/stamp.jsp?tp=arnumber=5710094, Accessed on: 2019-12-03

[33] Kim, K.-T.; Hur, J.; Kang, G.-H. Inter-turn fault analysis of IPM type BLDC motor using fault impedance modeling. In Proceedings of the 8th International Conference on Power Electronics—ECCE Asia, Jeju, Korea, 30 May–3 June 2011; pp. 2216–2224. [Online] Available :https://ieeexplore.ieee.org/stamp/stamp.jsp?tp=arnumber=5944430, Accessed on: 2019-12-03

[34] R. Z. Haddad and E. G. Strangas, "Detection of static eccentricity and turn-to-turn short circuit faults in permanent magnet synchronous AC machines," 2015 IEEE 10th International Symposium on Diagnostics for Electrical Machines, Power Electronics and Drives (SDEMPED), Guarda, 2015, pp. 277-283. [Online] Available :https://ieeexplore.ieee.org/stamp/stamp.jsp?tp=arnumber=7303702, Accessed on: 2019-12-03

[35] D. J. Gómez, A. L. Rodríguez, I. Villar, A. López-de-Heredia, I. Etxeberria-Otadui and Z. Q. Zhu, "Improved permeance network model for embedded magnet synchronous machines," 2014 International Conference on Electrical Machines (ICEM), Berlin, 2014, pp. 1231-1237. [Online] Available :https://ieeexplore.ieee.org/document/6960339, Accessed on: 2019-12-03

[36] B. Aubert, J. Régnier, S. Caux and D. Alejo, "Kalman-Filter-Based Indicator for Online Interturn Short Circuits Detection in Permanent-Magnet Synchronous Generators," in IEEE

Transactions on Industrial Electronics, vol. 62, no. 3, pp. 1921-1930, March 2015. [Online] Available :, Accessed on: 2019-12-03

[37] "Geometrical Permeance Network Based Real-Time Nonlinear Induction, Scott D. Sudhoff, Senior Member, IEEE, Brian T. Kuhn, Member, IEEE, Keith A. Corzine, Member, IEEE, and Brian T. Branecky", Accessed on: 2019-12-03

[38] B. Vaseghi, N. Takorabet and F. Meibody-Tabar, "Fault Analysis and Parameter Identification of Permanent-Magnet Motors by the Finite-Element Method," in IEEE Transactions on Magnetics, vol. 45, no. 9, pp. 3290-3295, Sept. 2009. [Online] Available :https://ieeexplore.ieee.org/stamp/stamp.jsp?tp=arnumber=5208493, Accessed on: 2019-12-03

[39] S. D. Sudhoff, B. T. Kuhn, K. A. Corzine and B. T. Branecky, "Magnetic Equivalent Circuit Modeling of Induction Motors," in IEEE Transactions on Energy Conversion, vol. 22, no. 2, pp. 259-270, June 2007. [Online] Available :https://ieeexplore.ieee.org/document/4207473, Accessed on: 2019-12-03

[40] M. Khov, J. Regnier and J. Faucher, "Monitoring of turn short-circuit faults in stator of PMSM in closed loop by on-line parameter estimation," 2009 IEEE International Symposium on Diagnostics for Electric Machines, Power Electronics and Drives, Cargese, 2009, pp. 1-6. [Online] Available :https://ieeexplore.ieee.org/stamp/stamp.jsp?tp=arnumber=5292797, Accessed on: 2019-12-03

[41] Pradhan, S.K.; Srivastava, R.K. Characterstics of stator inductances with intertum fault in PMBLDC motor using winding function approach. In Proceedings of the 2013 IEEE 1st International Conference on Condition Assessment Techniques in Electrical Systems (CATCON), Kolkata, India, 6–8 December 2013; pp. 139–144. [Online] Available :https://ieeexplore.ieee.org/stamp/stamp.jsp?tp=arnumber=6737487, Accessed on: 2019-12-03

[42] B. M. Ebrahimi and J. Faiz, "Feature Extraction for Short-Circuit Fault Detection in Permanent-Magnet Synchronous Motors Using Stator-Current Monitoring," in IEEE Transactions on Power Electronics, vol. 25, no. 10, pp. 2673-2682, Oct. 2010. [Online] Available :https://ieeexplore.ieee.org/stamp/stamp.jsp?tp=arnumber=5466244, Accessed on: 2019-12-03

[43] G. M. Joksimovic and J. Penman, "The detection of inter-turn short circuits in the stator windings of operating motors," in IEEE Transactions on Industrial Electronics, vol. 47, no. 5, pp. 1078-1084, Oct. 2000. [Online] Available :https://ieeexplore.ieee.org/stamp/stamp.jsp?tp=arnumber=873216, Accessed on: 2019-12-03

[44] J. Chai, J. Wang, K. Atallah and D. Howe, "Performance Comparison and Winding Fault Detection of Duplex 2-Phase and 3-Phase Fault-Tolerant Permanent Magnet Brushless Machines," 2007 IEEE Industry Applications Annual Meeting, New Orleans, LA, 2007, pp. 566-572. [Online] Available :https://ieeexplore.ieee.org/stamp/stamp.jsp?tp=arnumber=4347840, Accessed on: 2019-12-03

[45] S. Lee, K. Kim and J. Hur, "Diagnosis technique for stator winding inter-turn fault in BLDC motor using detection coil," 2015 9th International Conference on Power Electronics and ECCE Asia (ICPE-ECCE Asia), Seoul, 2015, pp. 2925-2931. [Online] Available :https://ieeexplore.ieee.org/stamp/stamp.jsp?tp=arnumber=7168191, Accessed on: 2019-12-03

[46] Julio-César Urresty, Jordi-Roger Riba, Luís Romeral, Application of the zero-sequence voltage component to detect stator winding inter-turn faults in PMSMs, Electric Power Systems Research, Volume 89, 2012, Pages 38-44. [Online] Available : https://doi.org/10.1016/j.epsr.2012.02.012., Accessed on: 2019-12-26

[47] C. Bouchareb and M. S. N. Saïd, "PMSM model with inter-turn fault," 2015 4th International Conference on Electrical Engineering (ICEE), Boumerdes, 2015, pp. 1-5. [Online] Available :https://ieeexplore.ieee.org/stamp/stamp.jsp?tp=arnumber=7416712, Accessed on: 2019-12-16

[48] P. Marissa, "5 Companies Who Succeed By Prioritizing Sustainability Over Profits,"Forbes, 12 Dec, 2017. [Online] Available :https://www.forbes.com/sites/marissaperetz/2017/12/12/5-

companies-who-succeed-by-prioritizing-sustainability-over-profits/153929dd5585, Accessed on: 2019-12-16

[49] S. Pokharel, "New Delhi is choking on smog and there's no end in sight," CNN, 4 Nov, 2019. [Online] Available : https://edition.cnn.com/2019/11/04/india/delhi-india-smog-pollution-intl-hnk/index.html, Accessed on: 2019-12-16

[50] K. Siddharth, "Is your phone tainted by the misery of the 35,000 children in Congo's mines?," The guardian, 12 Oct, 2018. [Online] Available : https://www.theguardian.com/global-development/2018/oct/12/phone-misery-children-congo-cobalt-mines-drc, Accessed on: 2019-12-16

[51] M. Enking, "Study: Climate change makes rich countries richer and poor ones poorer," grist, 23 Apr, 2019. [Online] Available : https://grist.org/article/study-climate-change-makes-rich-countries-richer-and-poor-ones-poorer/, Accessed on: 2019-12-17

A

Machine parameters

Table A.1: PMSM parameters

Parameter	**Value**
R_s	1.6 mΩ
L_s	292 μ H
M_s	-12 μ H
Ψ_m	0.068
Pole-pairs	5
f_0	125 Hz
Turns per phase	20
Coils per phase	4
Calculated inductances	
L_{coil}	88.423 μ H
M_{coil}	-5.141 μ H

Table A.2: Reference PMSM

Parameter	**Value**
R_s	0.44 Ω
L_s	2.82 mH
M_s	-0.28 mH
L_{a_1} @ $\mu_{coil} = 50$ %	1.62 mH
$M_{a_1a_2}$ @ $\mu_{coil} = 50$ %	-0.2 mh
L_{coil}	0.86 mH
M_{coil}	-0.05 mH
Pole-pairs	4